Bachelor's Thesis

Conventional superconductors in a magnetic field: The vortex state
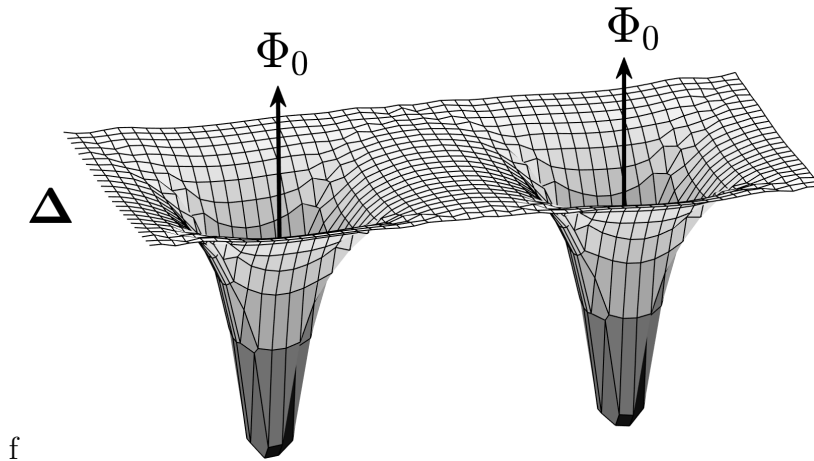
submitted by

Arya Prasetya

Matriculation Number : 3736281

May 14, 2021

To Uti,
For being the source of my drive in these last few months.
Engkau dirindukan.

To my family,
For the constant support, patience, and trust
given to me on this journey.

To Munir and Joan,
For the company, through ups and downs,
and being a home away from home.

Abstract

One of the most fundamental properties of a superconductor is its response to magnetic fields, such as its tendency to generate a counter-current that completely expels magnetic induction in the material. The study of a type-II superconductor, in particular, the vortex state when subject to a magnetic field is important for various practical applications. Therefore it is of interest to study the underlying mechanism behind it through the microscopic description. This thesis investigates properties of the vortex state of a superconductor from various viewpoints: 1) the phenomenological description (based on the London eq. and GL theory), and 2) the microscopic description of s-wave superconductivity (based on the tight binding model and BCS theory). Initially, some phenomenological description of the vortex state are presented and calculated through London equations and GL theory. The real-space microscopic description of a superconductor is then constructed from BCS theory and second quantization formalism. To do this, one uses the Bogoliubov-de Gennes equation to self consistently determine the superconducting order (gap) parameter. Implementation of magnetic fields in the system are done by introducing Peierls substitution and a gauge transformation in periodic boundary hoppings. With all the prerequisite knowledge, some phyisical parameters are numerically calculated to confirm that is indeed consistent with the phenomenological description. This includes the minimization of the free energy in the superconducting state, formation of the supercurrent, as well as flux pinning of vortices.

Declaration

Acknowledgements

Contents

Chapter 1

Introduction

1.1 What is Superconductivity?

In 1911, an experiment to study the resistance of pure mercury under low temperature was conducted by Kannerlingh Onnes. Due to Onnes' contributions in advancing the field of cryogenics, ambient temperatures at that time can be brought down to 1.5K through the liquefaction of helium. It was then discovered, that around 4.3K, the resistance of mercury abruptly drops to a value indistinguishable to zero [1].

This discovery became the conception of superconductivity. When passing below a critical temperature T_c, the superconducting phase can be characterized by two prominent physical properties. The first is perfect conductivity; the vanishing of resistance as discovered by Onnes, with further evidence shown by the capability of superconductors to produce a persistent current [2]. The second is perfect diamagnetism, which is the tendency for superconductors to form magnetic dipoles moments that opposes the applied external magnetic field known as the Meißner effect. As a consequence, magnetic flux is are also prevented from penetrating the interior of the superconducting material (see Fig. 1.1) [3].
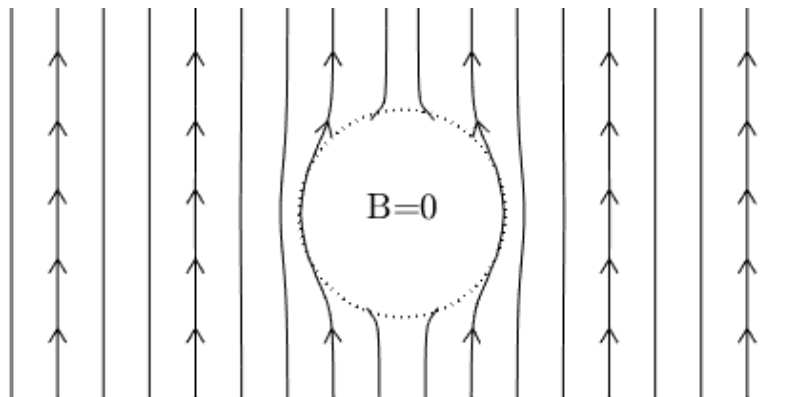
Figure 1.1: The Meißner effect: Under perfect diamagnetism, an opposing current generates a magnetic field that opposes the applied field.

Since then, superconductivity has become a well-known phase of solid-state matter. The macroscopic description has been well developed by London, Pippard, and

Ginzburg-Landau theory, while BCS theory has paved the way to the microscopic understanding of the phenomena. Nevertheless, there is still considerable interest in fundamental research within the field, particularly in the microscopic theory of high-T_c superconductors, which is yet to be found. The current practical application of superconductivity is broad, from usage in fault-current limiters to superconducting magnets in medical imaging [4]. Therefore, studying the behaviour of superconductors in various state variables, in particular magnetic fields, is of the utmost importance.

1.1.1   Phase transition in superconductivity

Before discussing superconductivity as a phase transition, we must first understand the concept of phase transitions.

From the macroscopic perspectives, we know that matter can take different states such as solid, liquid, and gas. These states can be distinguished in terms of the way the atoms within each matter are organized, positioned, and interact.

More precisely, the phase transition is then associated with the breaking of symmetries. In the case of liquid to solid, it is the breaking of the continuous translational and rotational symmetry. This occurs because particles in liquid possess a random position and orientation while particles in solid are fixed positions and orientations.

In the case of superconductivity, a phase transition exists due to the breaking of the global $U(1)$ gauge symmetry. This implies that the internal energy of the superconducting system is not invariant under a gauge transformation, which corresponds to a complex phase shift in the wave function [5].

The breaking of symmetries in many of these systems can be observed in order parameters. These are parameters that show whether a phase transition has occurred. For the case of a superconducting system it is the superconducting gap,

$$\Delta = V\langle c_\downarrow c_\uparrow \rangle, \quad V < 0 \tag{1.1}$$

where $c_\uparrow$ and $c_\downarrow$ are spin-dependent fermionic annihilation operators and $V < 0$ is an interaction constant. The expectation value of the fermionic annihilation operators along with its conjugate represent the formation of bound electrons called the Cooper pair.

Contrary to other order parameters, the gap is in general a complex quantity, due to the to the aforementioned symmetry breaking under gauge transformation of $c \to ce^{i\theta}$ on the expectation of annihilation operators. The usage of second quantized formalism will be introduced later in the chapter.

1.1.2   Type-II superconductors and the vortex state

In the five decades after the initial discovery of superconductivity, studies in the behaviour of superconducting alloys in magnetics has been intensively discussed and studied.
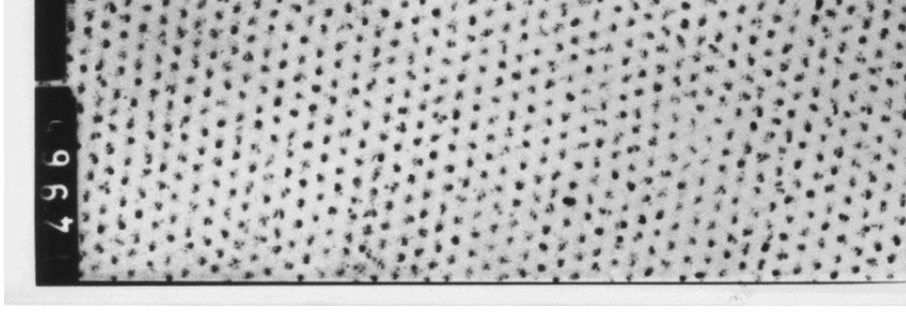
Figure 1.2: Flux lattice structure of a vortex state, observed through the deposition of ferromagnetic particles formed near a superconducting surface [12].

It was then experimentally shown by de Haas that a superconducting Bismuth wire possesses two critical fields, before the superconducting state is destroyed. The intermediate state where a slight increase followed by a constant trend of resistance, was initially thought to exist due to the inhomogeneity of the sample [6]. This explanation, however, proved to be flawed when Shubnikov showed that the two critical fields still exist accounting for the inhomogeneity of the sample [7],

In 1957, Abrikosov was able to explain this phenomenon through Ginzburg-Landau theory. He hypothesized that it is energetically favorable to form of magnetic flux through the superconducting material, causing the intermediate state [8]. The magnetic flux penetrates the superconductor with a discrete strength of a single flux quantum [9],

$$\Phi_0 = \frac{hc}{2e}_1.$$

(1.2)

Abrikosov also deduced that the magnetic flux forms a lattice structure which is experimentally confirmed by Essmann through direct observation (see Fig. 1.2). This prediction is completed by Kleiner's theoretical calculation showing that the equilibrium positions of the vortex state was found to take a hexagonal lattice structure [11], this is confirmed experimentally by Essmann [12]. This discovery becomes the basis of the type-II superconductors as well as the intermediate "vortex state".

In this thesis, we will explore the properties of conventional superconductors under a magnetic field, in particular, phenomena such as the vortex state. We will begin with the phenomenological descriptions of the superconducting state in magnetic fields. Afterward, the microscopic theory of conventional superconductors, based on the tight-binding model and the BCS theory in real-space. will be applied.

1.2   Second quantization

Since superconductivity turns out to be a phenomenon of quantum mechanics of many particle states of electrons that incorporate electron pairing interactions, a

---

[1]Intially, London's calculation defined the quantum flux as $\Phi_0 = \frac{hc}{e}$, but an experiment by Deaver and Fairbanks [10] has shown that it is $\Phi_0 = \frac{hc}{2e}$. This also shows early evidence of the Cooper pair.

microscopic description of a superconducting system can be constructed through quantum mechanics. To this end, it is convenient to utilize the second quantization formalism. This way we can describe many-particle systems without having to worry about the dynamics of every particle. Therefore, this formalism will be an important tool in the tight-binding model that will be used to describe superconductivity.

Second quantization hinges on two main grounds from quantum theory, which is the indistinguishability of particles and the ability to form a basis in the Hilbert space of N-particle state from single-particle states. Second quantization is explained extensively in many textbooks, he we will follow the discussion from "Many-body quantum theory in condensed matter physics" by Bruus and Flensberg [13]. Let's first conceptualize this from first quantization.

1.2.1 N-particle state and indistinguishability

We consider a complete orthonormal single-particle basis $\{\Psi_{\nu_i}(\mathbf{r})\}$, where ν is just some complete set of quantum numbers[2]. Additionally, we generate an N-particle state $\Psi(\mathbf{r}_1, \mathbf{r}_2, ..., \mathbf{r}_N)$. Using the orthonormality of the single-state function, we can obtain some $(N-1)$-particle function A_{ν_1} that can represent the N-particle state in terms of a single-particle state.

$$\Psi(\mathbf{r}_1', \mathbf{r}_2, ..., \mathbf{r}_N) = \sum_{\nu_1} \Psi_{\nu_1}(\mathbf{r}_1') A_{\nu_1}(\mathbf{r}_2, ..., \mathbf{r}_N) \tag{1.3}$$

A_{ν_1} can then be represented in terms of some $(N-2)$-particle function A_{ν_1, ν_2} in a similar manner. Continuing recursively N times, we will reach to the single-state basis representation of N-particle state, as a linear superposition of products that form a basis in the N-particle Hilbert space.

$$\Psi(\mathbf{r}_1, \mathbf{r}_2, ..., \mathbf{r}_N) = \sum_{\nu_1, ..., \nu_N} A_{\nu_1, ..., \nu_N} \prod_i^N \Psi_{\nu_i}(\mathbf{r}_i) \tag{1.4}$$

To obey the allowed symmetries under exchange of two particles, it turns out that there are distinct particle types of bosons and fermions. To incorporate explicit fermion symmetry one can introduce the anti-symmetrization operator, $\hat{S}_- = \det(\prod_i^N \Psi_{\nu_i}(\mathbf{r}_i))$. We obtain a symmetric basis, where only occupied single-state basis play a role [13].

$$\Psi(\mathbf{r}_1, \mathbf{r}_2, ..., \mathbf{r}_N) = \sum_{\nu_1, ..., \nu_N} B_{\nu_1, ..., \nu_N} \hat{S}_- \prod_i^N \Psi_{\nu_i}(\mathbf{r}_i) \tag{1.5}$$

Furthermore, the notion of indistinguishability of particles comes from the distinction between classical and quantum as pictured in Fig. 1.3.

Within classical mechanics, we can track identical particles given an initial condition of position and momentum. Lets say we have chosen the red particle, we can then follow the particle along the trajectory and distinguish one particle from another.

---

[2]For example, hydrogen orbital has $\nu = n, l, m, \sigma$.
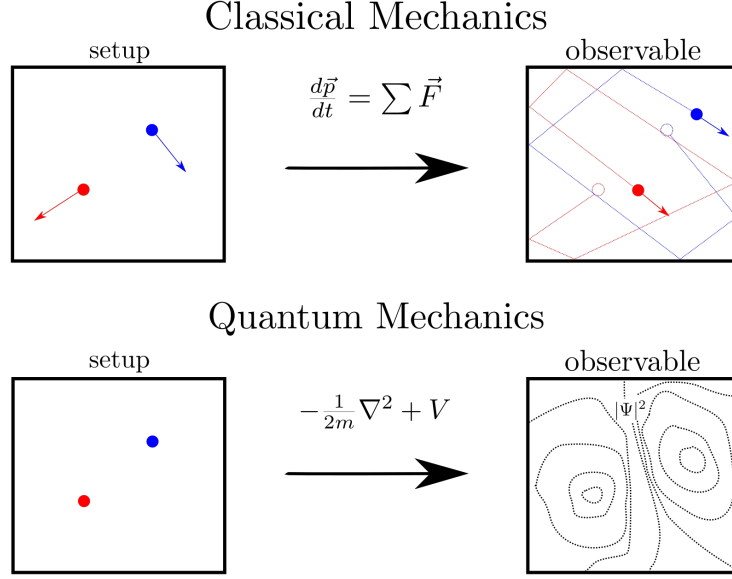
Figure 1.3: Indistinuishability in quantum mechanics

This however breaks down in quantum mechanics, as tracking the trajectory of a particle would violate Heisenberg's uncertainty principle, $\sigma_p\sigma_x \geq \hbar/2$, where σ_p and σ_x is the uncertainty of momentum and position respectively. As a consequence, what we can observe is a probability of where a particle might exist, without really knowing which particle is which. Referring back to Fig. 1.3, once we have chosen a point in space along the observables, one can only say that there is a superposition of red and blue particles rather than one distinct particle.

1.2.2 Second quantization for fermionic systems

With indistinguishable particles and a well-defined complete basis, we have justified in representing a simpler notation. This then leads to the occupation number representation basis state. For this thesis, it will be assumed from now on, that the occupation number $\nu = \{\mathbf{k} = (k_x, k_y), \sigma = \pm 1\}$, describing a free-electron particle in two dimensions, with spin up and spin down,

$$\left| n_{\mathbf{k}_1,\sigma}, n_{\mathbf{k}_2,\sigma}, n_{\mathbf{k}_3,\sigma}, ... \right\rangle, \tag{1.6}$$

where $N = \sum_{i,\sigma} n_{\mathbf{k}_i,\sigma}$ is the total number of particles in the system. According to the exclusion principle, occupation number has a value of $n_{\nu_i} = 0, 1$ for fermions. The space spanned by the basis is the Fock space $\bigoplus_N \mathcal{F}_N$, where $\mathcal{F}_N = \mathrm{span}(\left| n_{\mathbf{k}_1,\sigma}, n_{\mathbf{k}_2,\sigma}, n_{\mathbf{k}_3,\sigma}, ... \right\rangle \mid \sum_{i,\sigma} n_{\mathbf{k}_i,\sigma} = N)$ [13].

The formalism depends on two important operators, the creation and annihilation operator. Creation operator $c_{\mathbf{k},\sigma}^{\dagger}$ adds a particle in the occupation number ν, while the annihilation operator $c_{\mathbf{k},\sigma}$ removes a particle.

Since the Pauli exclusion principle has to be taken into account, an annihilation of a state with zero particle or a creation of particle in an occupied state vanishes. This

property are described in the following,

$$
\begin{aligned}
c_{\mathbf{k},\sigma} \ket{n_{\mathbf{k},\sigma}} &= \sqrt{n_{\mathbf{k},\sigma}} \ket{n_{\mathbf{k},\sigma} - 1}, \\
c_{\mathbf{k},\sigma}^{\dagger} \ket{n_{\mathbf{k},\sigma}} &= \sqrt{n_{\mathbf{k},\sigma} + 1} \ket{n_{\mathbf{k},\sigma} + 1}.
\end{aligned}
\tag{1.7}
$$

The number of particle $n_{\mathbf{k},\sigma}$ can then be found through the number operator,

$$
\hat{n}_{\mathbf{k},\sigma} = c_{\mathbf{k},\sigma}^{\dagger} c_{\mathbf{k},\sigma}.
\tag{1.8}
$$

Note that if we consider beyond non-zero temperature, statistical mechanics have to be taken into account and the number of particles have to follow the thermal average of the state, which is given by the Fermi distribution,

$$
\langle \hat{n}_{\mathbf{k},\sigma} \rangle = f(\epsilon_{\mathbf{k},\sigma}) = \frac{1}{1 + e^{\frac{1}{k_B T}(\epsilon_{\mathbf{k},\sigma} - \mu)}},
\tag{1.9}
$$

where a chemical potential μ is given as particle number is not conserved in a grand canonical ensemble.

The fermionic creation and annihilation operators then follow the anticommutator relations,

$$
\begin{aligned}
\{c_{\mathbf{k}_i,\sigma}^{\dagger}, c_{\mathbf{k}_j,\sigma'}\} &= \delta_{\mathbf{k}_i,\mathbf{k}_j} \delta_{\sigma,\sigma'}, \\
\{c_{\mathbf{k}_i,\sigma}, c_{\mathbf{k}_j,\sigma'}\} &= 0, \\
\{c_{\mathbf{k}_i,\sigma}^{\dagger}, c_{\mathbf{k}_j,\sigma'}^{\dagger}\} &= 0,
\end{aligned}
\tag{1.10}
$$

where $\{A, B\} = AB + BA$.

It is also useful to extend the representation to real-space by using the quantum field operator $\Psi_\sigma(\mathbf{r})$. Using the Fourier transform of the reciprocal-space, one can then find the relation,

$$
\begin{aligned}
\Psi_\sigma^{\dagger}(\mathbf{r}) &= \sum_{\mathbf{k}} \langle \mathbf{k}, \sigma | \mathbf{r}, \sigma \rangle c_{\mathbf{k},\sigma}^{\dagger}, \\
c_{\mathbf{k},\sigma}^{\dagger} &= \int d\mathbf{r} \, \langle \mathbf{r}, \sigma | \mathbf{k}, \sigma \rangle \Psi_\sigma^{\dagger}(\mathbf{r}), \\
\langle \mathbf{r}, \sigma | \mathbf{k}, \sigma \rangle &= \frac{1}{\sqrt{\Omega}} e^{i\mathbf{k}\cdot\mathbf{r}},
\end{aligned}
\tag{1.11}
$$

with Ω being the system size, specifically $\Omega = N$ for an N-particle system.

Chapter 2

Phenomenological description of superconductivity

2.1 Magnetic field calculations through London equation

The London equations are one of the first attempts to describe the superconducting phenomena found in the Meißner-Ochsenfeld effect through the dynamics of a supercurrent $\mathbf{J}_\mathrm{s}$ under electromagnetic fields [14],

$$
\begin{aligned}
\partial_t(\Lambda \mathbf{J}_\mathrm{s}) &= \mathbf{E} \\
c\boldsymbol{\nabla} \times \Lambda \mathbf{J}_\mathrm{s} &= -\mathbf{B} \\
\Lambda &= \frac{m}{n_\mathrm{s} e^2}
\end{aligned}
\tag{2.1}
$$

where "acceleration" constant Λ is the value at which the supercurrent evolves, that depends on the number density of superconducting electrons n_s, elementary charge e, and electronic mass m. In this chapter, Tinkham's discussion on the applications of this equation in the phenomenological description will be followed [15].

While the first London equation describes the influence of an electric field towards electrons in a supercurrent, the second equation carries a physical significance, as it shows that the propagating supercurrent in a material gives rise to an opposing magnetic field that contributes to the perfect diamagnetism in superconductors.

The form of the London equation is motivated by the fact that the lowest electronic free energy corresponds to a zero net current [16]. By carrying this over to the canonical momentum of an electron in an electromagnetic field, $m\mathbf{v} + e\mathbf{A}/c$, one obtains an average drift velocity of the current and hence also the supercurrent,

$$
\mathbf{J}_\mathbf{s} = n_\mathrm{s} e \langle \mathbf{v}_\mathrm{s} \rangle = -\frac{n_\mathrm{s} e^2}{mc} \mathbf{A} = -\frac{1}{\Lambda c} \mathbf{A}
\tag{2.2}
$$

This relation is also known as the London gauge. Taking the curl of Eq. (2.2) leads to the London equations [15].

Using Ampere's law in Maxwell's equation, $4\pi/c\mathbf{J_s} = \boldsymbol{\nabla} \times \mathbf{B}$ (Gaussian units), the

magnetic profile of a superconducting material can be deduced.

$$\mathbf{B} = -\lambda^2 \boldsymbol{\nabla} \times \boldsymbol{\nabla} \times \mathbf{B}$$
$$= \lambda^2 \nabla^2 \mathbf{B} \tag{2.3}$$

The second order differential equation of the magnetic field is obtained by a simple vector identity and then noting that Maxwell's equation does not permit the existence of magnetic monopoles $\boldsymbol{\nabla} \cdot \mathbf{B} = 0$. This then gives a solution, where magnetic field decays exponentially as one get further from the superconducting surface, inside the material. The attenuation of the magnetic field is characterized by the penetration depth $\lambda^2 = c^2 \Lambda/(4\pi)$.

Furthermore, by assuming a steady supercurrent, we can also show by Helmholtz's theorem that the superconducting state does not obey Ohm's law. This is an important point, as it distinguishes a superconductor to an ideal conductor (see Appendix A.1).

2.1.1 Magnetic field of a superconducting slab

To show the application of London equations, we consider a superconducting slab of length d, with a uniformly applied field $\mathbf{B}_\mathrm{a}$.
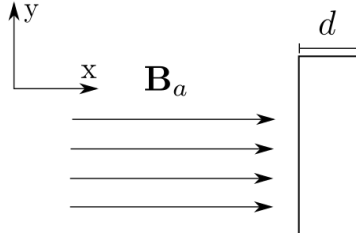
Figure 2.1: Uniform field on a superconducting slab.

We can reduce this into a simple 1D boundary-value problem. For convenience, we will set our origin in the middle of the slab.

Taking the expected magnetic profile (Eq. 2.3), we can propose the ansatz for 1D to be,

$$B_\mathrm{x}(x) = C_+ e^{\frac{x}{\lambda}} + C_- e^{-\frac{x}{\lambda}}. \tag{2.4}$$

Since the minimum of the magnetic field should be located in the middle of the slab, we can deduce,

$$\frac{dB_\mathrm{x}}{dx}(0) = 0 = C_+ - C_-$$
$$\Rightarrow C = C_+ = C_- \tag{2.5}$$
$$\Rightarrow B_\mathrm{x}(x) = 2C \cosh \frac{x}{\lambda}.$$

It is known that there exist no attenuation of field outside the superconducting material, therefore,

$$B_\mathrm{a} = B_\mathrm{x}\left(-\frac{d}{2}\right) = B_x\left(\frac{d}{2}\right)$$
$$\Rightarrow B_\mathrm{a} = C \cosh \frac{d}{2\lambda}. \tag{2.6}$$

With the formula above, one can produce through simple electrodynamics the magnetic field profile of a superconducting material.

$$\mathbf{B}(x) = \begin{cases} B_{\mathrm{a}} \frac{\cosh x/\lambda}{\cosh d/(2\lambda)} \mathbf{e}_{\mathrm{x}} & \text{if } |x| < \frac{d}{2} \\ B_{\mathrm{a}} \mathbf{e}_{\mathrm{x}} & \text{else} \end{cases} \tag{2.7}$$

Recalling that $\lambda^2 \propto \frac{1}{n_{\mathrm{s}}}$, we can also see that the more superconducting electrons exists, the faster the magnetic field drops to zero, since the hyperbolic prefactor exponentially increases with lower penetration depth.

2.2 Vortex lattice

The superconducting characteristic of a material is determined by the GL parameter κ given by,

$$\kappa = \frac{\lambda}{\xi}. \tag{2.8}$$

For $\kappa \leq \frac{1}{\sqrt{2}}$ it is a type-I superconductor, characterized by the Meißner effect. While for $\kappa > \frac{1}{\sqrt{2}}$ one obtains a type-II superconductor. The coherence length ξ is a parameter that determines the length scale of interactions between electrons, which is associated to the formation of Cooper pairs [15]. To phenomenologically obtain ξ, one can use the Ginzburg-Landau theory which is discussed in Appendix B. In addition to this, ξ can also be determined microscopically by studying the spatial variation of the superconducting order (gap) parameter, as we will see in Chapter 4.

When field densities are in the range of $\Phi_0/\lambda^2 \lesssim B_{\mathrm{a}} \ll \Phi_0/\xi^2$, the intermediate vortex state forms a periodic lattice, where there will be integer numbers of flux quantum Φ_0 adding up to the external magnetic field B_{a}. We will therefore investigate the field distribution as well as the reason behind its underlying lattice structure in nature.

2.2.1 Periodic structure and reciprocal lattice

To describe periodic structures, such as the vortex lattice, it is convenient to use primitive lattice vectors $\mathbf{a}_i \in \{1, 2\}$, where each lattice site can be described as integer sums of these vectors. In this section, we will investigate vortices for square and hexagonal lattice structures, with the following primitive vectors,

$$\mathbf{a}_i = a\mathbf{e}_i, \quad i = 1, 2 \tag{2.9}$$

for square lattice and,

$$\mathbf{a}_1 = a\mathbf{e}_1$$
$$\mathbf{a}_2 = \frac{a}{2}\mathbf{e}_1 + \frac{\sqrt{3}a}{2}\mathbf{e}_2 \tag{2.10}$$

for a hexagonal lattice, where a is the lattice constant of the system.
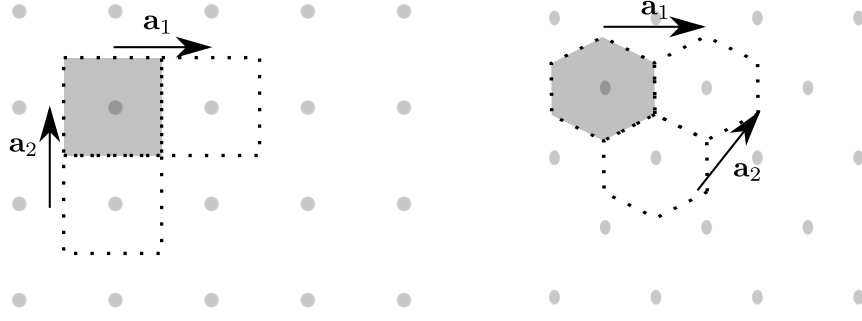
Figure 2.2: Unit cells of square and hexagonal lattice can periodically represent systems

From this, every point in the lattice can be written as a superposition of the primitive vectors,

$$\mathbf{r}_i = n_i\mathbf{a}_1 + m_i\mathbf{a}_2 \tag{2.11}$$

where i is a lattice site of coordinate $\{n_i, m_i\}$.

Analogously, due to periodicity, one can define the reciprocral lattice,

$$\mathbf{Q}_i = h_i\mathbf{b}_1 + k_i\mathbf{b}_2 \tag{2.12}$$

with the constraint $e^{i\mathbf{Q}_i \cdot \mathbf{r}_j} = 1$ and $\mathbf{a}_i \cdot \mathbf{b}_j = 2\pi\delta_{ij}$[17]. One then finds the reciprocal vectors to be,

$$\mathbf{b}_{\mathrm{i}} = \frac{2\pi}{a}\mathbf{e}_i, \quad i = 1, 2 \tag{2.13}$$

and,

$$\mathbf{b}_1 = \frac{2\pi}{a}(\mathbf{e}_1 - \frac{1}{\sqrt{3}}\mathbf{e}_2)$$
$$\mathbf{b}_2 = \frac{2\pi}{a}\frac{2}{\sqrt{3}}\mathbf{e}_2 \tag{2.14}$$

for the square and hexagonal lattice respectively.

The primitive lattice vectors will now also allow us to construct unit cells, which are elementary components of the entire system, that possesses translationally-symmetric properties, due to the periodicity. A general rule to construct the unit cell is to draw perpendicular lines at the midpoints of two lattice sites, generally defined by the primitive vectors, until one forms a closed geometry.

2.2.2 Vortex lattice field distribution

In studying the field distribution $\mathbf{B}$ of a vortex lattice, the field distribution can be found by solving the vortex wavefunction $\Psi = \Psi_\infty f(r)e^{i\theta}$ using the limiting case $r \to 0$ on the Ginzburg Landau equation [15], whereby $f(r)$ will take the form of,

$$f \approx \tanh\left(\frac{r}{\xi}\right). \tag{2.15}$$

We can see that with the approximation, $f(r)$ saturates to 1 as $r \to \infty$. Under a high κ-approximation ($\lambda \gg \xi$), the coherence length becomes relatively short such that $f \approx 1$ except for the vortex centers.

In the presence of vortex cores, the right hand side of the London equation acquires a sum over Dirac delta functions,

$$\mathbf{B} - \lambda^2 \nabla^2 \mathbf{B} = \Phi_0 \sum_i \delta^{(2)}(\mathbf{r} - \mathbf{r}_i)\mathbf{e}_z, \tag{2.16}$$

where each delta function describes a single flux quantum placed at the respective lattice sites. We can perform a Fourier analysis to take into account neighboring interactions between vortices. The field is then written as a Fourier series,

$$\mathbf{B}(\mathbf{r}) = \sum_j B(\mathbf{Q}_j)e^{i\mathbf{Q}_j \cdot \mathbf{r}}\mathbf{e}_z$$

$$\delta^{(2)}(\mathbf{r} - \mathbf{r}_k) = \frac{N}{\Omega} \sum_j e^{i\mathbf{Q}_j \cdot \mathbf{r}}\mathbf{e}_z. \tag{2.17}$$

In here, Ω is the system size, which is the total area of unit cells, where a single unit cell has an area of $\frac{\Phi_0}{B_a}$. Therefore $\Omega = \frac{\Phi_0 N}{B_a}$, where N is the number of lattice sites. Inserting Eq. (2.17) to Eq. (2.16), one obtains the following relation in the z-component,

$$\sum_j [B(\mathbf{Q}_j) + \lambda^2 \mathbf{Q}_j^2 B(\mathbf{Q}_j)]e^{i\mathbf{Q}_j \cdot \mathbf{r}} = B_a \sum_j e^{i\mathbf{Q}_j \cdot \mathbf{r}}. \tag{2.18}$$

Comparing coefficients of each complex term helps us to determine the coefficient $B(\mathbf{Q}_i)$ of the field densitiy Fourier series. This leads to the field distribution in real space,

$$\mathbf{B}(\mathbf{r}) = B_a \sum_j \frac{e^{i\mathbf{Q}_j \cdot \mathbf{r}}}{1 + \lambda^2 \mathbf{Q}_j^2}\mathbf{e}_z. \tag{2.19}$$
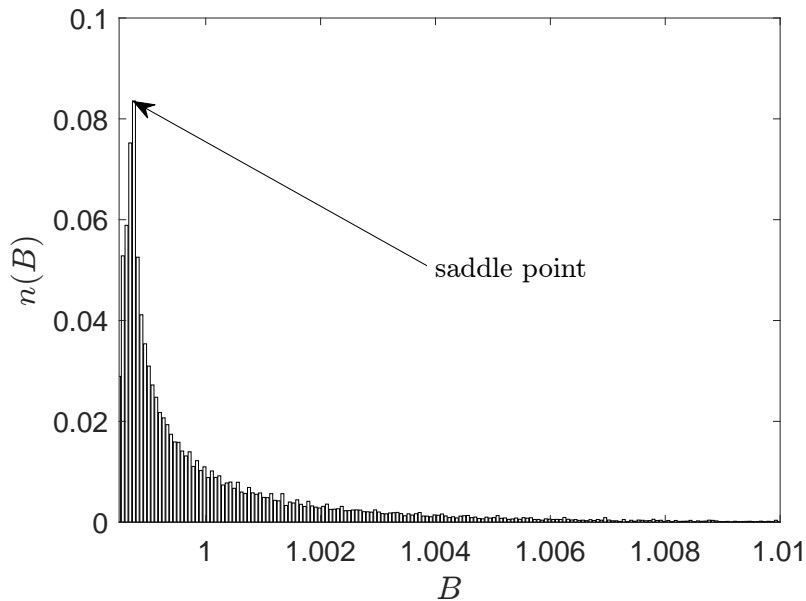
Figure 2.3: Field histogram of a hexagonal lattice, $\lambda = 5$, $B_a = 1$

By numerically evaluating Eq. (2.19), one can observe in particular the lattice structure. The details and figures are presented in Appendix C.1.

It is also interesting to point out that from the saddle point of the field distribution, one obtains a peak in the field histogram, corresponding to a van Hove singularity (see Fig. 2.3). This is analogous to those obtained in the density of states of electronic systems.

2.2.3 Free energy of field lattice structures

Given the magnetic field, one can calculate the change in free energy per unit length $f - f_{s0}$, where f_{s0} is the free energy of a superconductor in absence of vortices. This is useful to find the smallest free energy needed to form a vortex state, which may help explain the lattice structure found in nature.

We shall first begin by calculating the free energy for a single vortex. This is obtained through the energy of the magnetic fields and substracting away contributions from the kinetic energy of currents from the vortex, excluding the core [15],

$$\left.\frac{F - F_{s0}}{L}\right|_{\text{single vortex}} = \underbrace{\frac{1}{8\pi} \int_{0 < |\mathbf{r}| \leq r'} d^2\mathbf{r}\, \mathbf{H} \cdot \mathbf{B}}_{f_{\text{field}}} - \underbrace{\frac{1}{2c} \int_{0 < |\mathbf{r}| \leq r'} d^2\mathbf{r}\, \mathbf{J}_s \cdot \mathbf{A}_s}_{f_{\text{current}}} \tag{2.20}$$

$$= \frac{1}{8\pi} \int_{0 < |\mathbf{r}| \leq r'} d^2\mathbf{r}(\mathbf{B}^2 + 4\pi\Lambda\mathbf{J}_s^2).$$

In the above, magnetic permeability $\mu = 1$ was assumed. In Gaussian units, this implies $\mathbf{H} = \mathbf{B}$.

The vector potential is related by the London gauge $\mathbf{J}_s = (\Lambda c)^{-1}\mathbf{A}_s$ [Eq. (2.2)]. Using the Maxwell's equation on the supercurrent, the free energy can be written in terms of the magnetic field $\mathbf{B}$ and penetration depth λ,

$$\left.\frac{F - F_{s0}}{L}\right|_{\text{single vortex}} = \frac{1}{8\pi} \int_{0 < |\mathbf{r}| \leq r'} d^2\mathbf{r}[\mathbf{B}^2 + \lambda^2(\boldsymbol{\nabla} \times \mathbf{B})^2], \tag{2.21}$$

To solve this one would need the field distribution of a single vortex. One can use the modified London equations similar to Eq. (2.16) for a single vortex placed at the origin,

$$\mathbf{B} - \lambda^2\nabla^2\mathbf{B} = \Phi_0\delta^{(2)}(\mathbf{r})\mathbf{e}_z. \tag{2.22}$$

This differential equation has an exact solution,

$$B_z(\mathbf{r}) = \frac{\Phi_0}{2\pi\lambda^2}K_0\left(\frac{|\mathbf{r}|}{\lambda}\right), \tag{2.23}$$

where K_0 is the zeroth-order Hankel function, which has two limiting forms,

$$K_0\left(\frac{|\mathbf{r}|}{\lambda}\right) = \begin{cases} \left(\frac{\pi}{2}\frac{\lambda}{|\mathbf{r}|}\right)^{\frac{1}{2}} e^{-\frac{|\mathbf{r}|}{\lambda}} & |\mathbf{r}| \to \infty, \\ \left(\ln\frac{\lambda}{|\mathbf{r}|} + 0.12\right) & \xi \ll |\mathbf{r}| \ll \lambda. \end{cases} \tag{2.24}$$
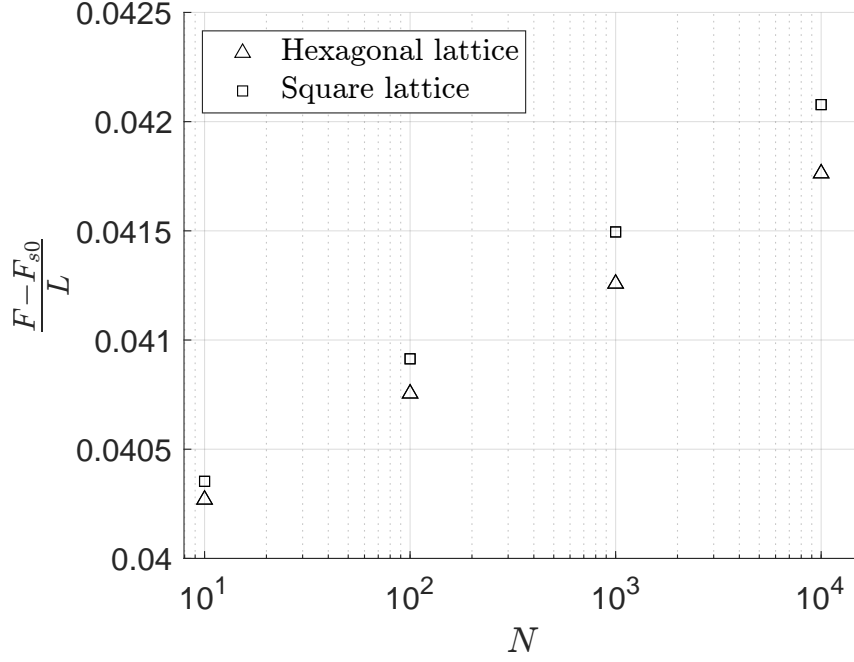
Figure 2.4: Free energies per unit length of different system sizes, $\lambda = 5$, $B_\mathrm{a} = 1$.

With the use of some vector calculus identities, we can transform the integral of Eq. (2.21). Please refer to Appendix A.2 for details of the derivation. Additionally, one can insert Eq. (2.22) to first term in the following to obtain a simpler integral.

$$
\begin{aligned}
\frac{F - F_\mathrm{s0}}{L}\bigg|_\mathrm{s.v.} &= \frac{1}{8\pi} \int_{0 < |\mathbf{r}| \leq r'} d^2\mathbf{r}(\mathbf{B} + \lambda^2 \boldsymbol{\nabla} \times \boldsymbol{\nabla} \times \mathbf{B}) \cdot \mathbf{B} + \frac{\lambda^2}{8\pi} \oint ds(\mathbf{B} \times \boldsymbol{\nabla} \times \mathbf{B}) \cdot \mathbf{e}_\mathrm{r} \\
&= \frac{1}{8\pi} \int_{0 < |\mathbf{r}| \leq r'} d^2\mathbf{r}|\mathbf{B}|\Phi_0 \delta^{(2)}(\mathbf{r}) + \frac{\lambda^2}{8\pi} \oint_{|\mathbf{r}| = r'} ds(\mathbf{B} \times \boldsymbol{\nabla} \times \mathbf{B}) \cdot \mathbf{e}_\mathrm{r}.
\end{aligned}
\tag{2.25}
$$

where, $\mathbf{e}_\mathrm{r}$ is just the radial unit vector in cylindrical coordinates. In the equation above, the first term just goes to zero since the core is excluded. This leaves us with the second term, which is just a closed line integral encircling the core at a radius r'. Evaluating the integral gives us,

$$
\frac{F - F_\mathrm{s0}}{L}\bigg|_\text{single vortex} = \frac{\lambda^2}{8\pi}\left[B_\mathrm{z}\frac{dB_\mathrm{z}}{dr}2\pi r\right]_{r'}.
\tag{2.26}
$$

According to Eq. (2.24), the free energy vanishes as $r' \to \infty$. However, it does give a finite contribution encircling the core $r' \approx \xi$. From this, one gets a value of,

$$
\frac{F - F_\mathrm{s0}}{L}\bigg|_\text{single vortex} = \frac{\Phi_0}{8\pi}B_\mathrm{z}(\xi) \approx \frac{\Phi_0}{8\pi}B_\mathrm{z}(0),
\tag{2.27}
$$

Extending this to multiple vortices, the fields are just superpositions of multiple single vortices, $\mathbf{B}(\mathbf{r}) = \sum_i B_z(|\mathbf{r} - \mathbf{r}_i|)\mathbf{e}_z$. Using this to calculate the free energy one obtains,

$$
\frac{F - F_\mathrm{s0}}{L} = \frac{\Phi_0}{8\pi}\left(\sum_i B_\mathrm{z,i}(\mathbf{r}_i) + \sum_{i \neq j} B_\mathrm{z,i}(\mathbf{r}_j)\right),
\tag{2.28}
$$

13

where interaction energy $i \neq j$ are obtained from the first term in Eq. (2.25) as delta functions may exist outside the core. Nevertheless, for large enough lattice constants, this term also vanishes due to the zeroth-order Hankel function at $|\mathbf{r}| \to \infty$. Due to periodicity, the on-site terms can be written as the same values $B_{z,i}(\mathbf{r}_i) = B_z(0)$. In addition to that, since there are B_a/Φ_0 vortices per unit area, we finally obtain the change in free energy for a vortex lattice,

$$\frac{F - F_{s0}}{L} = \frac{B_a B_z(0)}{8\pi} = \frac{B_a^2}{8\pi} \sum_i \frac{1}{1 + \lambda^2 \mathbf{Q}_i^2}. \tag{2.29}$$

The right-hand-side is given by inserting Eq. (2.19). To find the lattice structure that is realized in nature, one can impose different lattice structures and calculate the free energy by evaluating the sum over the reciprocal lattice vectors $\{\mathbf{Q}\}$.

By observing the change in free energy of different structures along varying system sizes (see Fig. 2.4), one can also validate Essmann's observation of its hexagonal lattice structure [12].

Chapter 3

From normal metal to superconductivity

3.1 Microscopic descriptions of normal metal

In general, when one wants to describe the electron dynamics for a condensed matter system, one should consider the Hamiltonian $\hat{H}$ in terms of the quantum field operators $\Psi_\sigma(\mathbf{r})$,

$$\hat{H} = \sum_\sigma \hat{H}_{0,\sigma} + \sum_{\sigma,\sigma'} \hat{V}_{\text{ee},\sigma\sigma'}$$

$$\hat{H}_{0,\sigma} = \int d^2\mathbf{r}\Psi_\sigma^\dagger(\mathbf{r})h(\mathbf{r})\Psi_\sigma(\mathbf{r}) \tag{3.1}$$

$$\hat{V}_{\text{ee},\sigma\sigma'} = \frac{1}{2} \iint d^2\mathbf{r}d^2\mathbf{r}'V_{\text{ee}}(\mathbf{r},\mathbf{r}')\Psi_\sigma^\dagger(\mathbf{r})\Psi_{\sigma'}^\dagger(\mathbf{r}')\Psi_{\sigma'}(\mathbf{r}')\Psi_\sigma(\mathbf{r}).$$

In this Hamiltonian, $h(\mathbf{r})$ is the atomic interaction from the Schrödinger equation. Meanwhile, $V_{\text{ee}}(\mathbf{r},\mathbf{r}')$ is the electronic interaction between particles [18].

In this section, we will explore further in depth on how one may treat such Hamiltonian in the second quantization formalism. This includes approximations such as the tight binding model for the atomic interactions. We shall also explore the effects of magnetic fields in a normal metal using the so-called Peierls substitution. For the purpose of this thesis, electronic interactions will be treated in the following section about superconductivity, to which the reason will be clear later.

3.1.1 The tight-binding model

In the tight-binding model, electronic wavefunctions are bounded to the lattice centers of its atoms. This allows us to expand the quantum field operators in a local basis that reflects the states of each isolated atoms, called the Wannier basis,

$$\Psi_\sigma(\mathbf{r}) = \sum_i^N \phi(\mathbf{r} - \mathbf{r}_i)c_{i\sigma}, \tag{3.2}$$

where each basis are localized at lattice site position $\mathbf{r}_i$ over $N = L_{\mathrm{x}}L_{\mathrm{y}}$ sites. Following our assumptions that the Wannier functions $\phi(\mathbf{r} - \mathbf{r}_i)$ are bounded to each lattice, they are then orthonormal,

$$\int d^2\mathbf{r}\phi^*(\mathbf{r} - \mathbf{r}_i)\phi(\mathbf{r} - \mathbf{r}_j) = \delta_{ij} \tag{3.3}$$

Additionally the Fourier transformation to the momentum space is then constrained to the Brillouin zones, such that the annihilation operator at site i is given by,

$$c_{i\sigma} = \frac{1}{\sqrt{N}} \sum_{\mathbf{k} \in \text{B.Z.}} e^{-i\mathbf{k}\cdot\mathbf{r}_i}c_{\mathbf{k}\sigma}. \tag{3.4}$$

From the above, one can the show that the anticommutation relations follows,

$$\begin{aligned}
\{c_{i\sigma}^\dagger, c_{j\sigma'}\} &= \delta_{ij}\delta_{\sigma\sigma'} \\
\{c_{i\sigma}, c_{j\sigma'}\} &= 0 \\
\{c_{i\sigma}^\dagger, c_{j\sigma'}^\dagger\} &= 0.
\end{aligned} \tag{3.5}$$

The reader is referred to Appendix A.4 for details of the derivation.

Furthermore, we have two considerations when treating electrons in a metal using the tight binding model. Firstly, the Born-von-Karman boundary condition is used to approximate invariance in lattice translation in large systems. In here, one imposes $e^{i\mathbf{k}\cdot L_n\mathbf{a}_n}\Psi(\mathbf{r}) = \Psi(\mathbf{r}+L_n\mathbf{a}_n)$, in particular $e^{i\mathbf{k}\cdot L_n\mathbf{a}_n} = 1$, $n = \mathrm{x}, \mathrm{y}$ where L_n is the length of the lattice at the direction of primitve unit vector $\mathbf{a}_n$. Periodicity is induced by setting $\mathbf{k} \cdot L_n\mathbf{a}_n = 2\pi m$, where $m \in \mathbb{Z}$. Then one uses the Born-Oppenheimer approximation to fix the position of the nuclei, treating them as "frozen phonons" [17].

With the considerations above, we shall evaluate the dynamics of an electron in a 2-dimensional lattice. To simplify the problem, we will consider a square lattice structure. The atomic interaction from the Schrödinger equation of such a system is then the following,

$$\begin{aligned}
h(\mathbf{r}) &= \frac{\mathbf{p}^2}{2m} + \sum_i^N V(\mathbf{r} - \mathbf{r}_i) \\
&= -\frac{\hbar^2}{2m}\boldsymbol{\nabla}^2 + \sum_i^N V(\mathbf{r} - \mathbf{r}_i).
\end{aligned} \tag{3.6}$$

The lattice potential $V(\mathbf{r} - \mathbf{r}_i)$ is a interaction between stationary nucleus and the electron which rapidly vanishes away from the lattice centers. Inserting the Wannier basis into the atomic interaction term in Eq. (3.1) leads us to a general second quantization form of the term,

$$\begin{aligned}
\hat{H}_{0,\sigma} &= -\frac{\hbar^2}{2m}\sum_{i,j}^N \int d^2\mathbf{r}\phi^*(\mathbf{r} - \mathbf{r}_i)\boldsymbol{\nabla}^2\phi(\mathbf{r} - \mathbf{r}_j)c_{i\sigma}^\dagger c_{j\sigma} \\
&\quad + \sum_i^N \int d^2\mathbf{r}\phi^*(\mathbf{r} - \mathbf{r}_i)V(\mathbf{r} - \mathbf{r}_i)\phi(\mathbf{r} - \mathbf{r}_i)c_{i\sigma}^\dagger c_{i\sigma}.
\end{aligned} \tag{3.7}$$

With the help of the finite-difference approximation, one can compute the first term in Eq. (3.7) as a 3-point approximated Laplacian,

$$
\begin{aligned}
\nabla^2\phi(\mathbf{r}) = &\frac{1}{a^2}[\phi(\mathbf{r} - \mathbf{a}_{\mathrm{x}}) + \phi_\sigma(\mathbf{r} - \mathbf{a}_{\mathrm{y}}) - 4\phi(\mathbf{r}) \\
&+ \phi(\mathbf{r} + \mathbf{a}_{\mathrm{x}}) + \phi(\mathbf{r} + \mathbf{a}_{\mathrm{y}})].
\end{aligned}
\tag{3.8}
$$

See Appendix A.3 for details of the finite-difference approximation.

By noticing that the approximation gives 4 wavefunction shifted by a single primitive unit vector and a single on-site wavefunction, we obtain the tight-binding Hamiltonian for nearest neighbor interactions in second quantization formalism,

$$
\hat{H}_{0,\sigma} = -\sum_{\langle i,j \rangle}^{N} t_{ij} c_{i\sigma}^\dagger c_{j\sigma} - \mu \sum_i^N c_{i\sigma}^\dagger c_{i\sigma},
\tag{3.9}
$$

where the t_{ij} is the hopping integral, which tell us the energy at which an electron "hops" from one lattice site to another. The on-site term is the chemical potential μ, associated with the interactions between electrons and its atoms. More explicitly this is given by

$$
t_{ij} = \int d^2\mathbf{r}\phi^*(\mathbf{r} - \mathbf{r}_i) \left[t\nabla^2 - \sum_k^N V(\mathbf{r} - \mathbf{r}_k) \right] \phi(\mathbf{r} - \mathbf{r}_j).
\tag{3.10}
$$

$$
\mu = t_{ii}.
$$

In the hopping integrals, we have set the hopping parameter $t = \frac{\hbar}{2ma^2}$. Using the orthonormality of the Wannier wavefunctions and the approximation that $V(\mathbf{r} - \mathbf{r}_k)$ vanishes rapidly away atomic centers $\mathbf{r}_k$, we find that $t_{ij} = t$ and $\mu = -4t - V_0$, where V_0 is the ground-state energy of the atoms in the system.

With the Hamiltonian of the nearest neighbor tight-binding model found, it is convenient to use its matrix representation, in terms of the vector form of the creation/annihilation operators $\mathbf{c}^\dagger = (c_1^\dagger, c_2^\dagger, ..c_N^\dagger)$ and $\mathbf{c} = (c_1, c_2, ..c_N)^{\mathrm{T}}$, where $\hat{H}_{0,\sigma} = \mathbf{c}_\sigma^\dagger H_{0,\sigma} \mathbf{c}_\sigma$. As an example, the matrix representation of 3×3 lattice takes the form,

$$
H_{0,\sigma} = \begin{pmatrix}
-\mu & -t_{12} & -t_{13} & -t_{14} & 0 & 0 & -t_{17} & 0 & 0 \\
-t_{21} & -\mu & -t_{23} & 0 & -t_{25} & 0 & 0 & -t_{28} & 0 \\
-t_{31} & -t_{32} & -\mu & 0 & 0 & -t_{36} & 0 & 0 & -t_{39} \\
-t_{41} & 0 & 0 & -\mu & -t_{45} & -t_{46} & -t_{47} & 0 & 0 \\
0 & -t_{52} & 0 & -t_{54} & -\mu & -t_{56} & 0 & -t_{58} & 0 \\
0 & 0 & -t_{63} & -t_{64} & -t_{65} & -\mu & 0 & 0 & -t_{69} \\
-t_{71} & 0 & 0 & -t_{74} & 0 & 0 & -\mu & -t_{78} & -t_{79} \\
0 & -t_{82} & 0 & 0 & -t_{85} & 0 & -t_{87} & -\mu & -t_{89} \\
0 & 0 & -t_{93} & 0 & 0 & -t_{96} & -t_{97} & -t_{98} & -\mu
\end{pmatrix},
\tag{3.11}
$$

where the hopping integrals t_{ij} inside the 3×3 block matrix along the diagonal represent hoppings along the x-direction, while the hopping integrals inside the 3×3 block matrix along the off-diagonal represent hoppings along the y-direction.

To find the eigenenergy E_i of the Hamiltonian above, one can use the property of the Hermitian matrix to generate an eigenstate from some unitary matrix U, such that $D = U^* H_{0,\sigma} U$ and $\text{diag}(D) = \{E_i\}$.

Analogously, the diagonalization of the Hamiltonian can also be obtained by Fourier transforming the Hamiltonian to its momentum-space representation. By inserting the corresponding momentum Fourier representations of the annihilation and creation operator in Eq. (3.4) for lattice size $N = L_x L_y$,

$$
\begin{aligned}
\hat{H}_{0,\sigma} &= -\sum_{\langle i,j \rangle}^{N} t_{ij} c_{i\sigma}^\dagger c_{j\sigma} - \mu \sum_{i}^{N} c_{i\sigma}^\dagger c_{i\sigma} \\
&= -\frac{t}{N} \sum_{\langle i,j \rangle}^{N} \sum_{\mathbf{k},\mathbf{k}' \in \text{B.Z.}} e^{i(\mathbf{k} \cdot \mathbf{r}_i - \mathbf{k}' \cdot \mathbf{r}_j)} c_{\mathbf{k}}^\dagger c_{\mathbf{k}'} - \frac{\mu}{N} \sum_{i}^{N} \sum_{\mathbf{k},\mathbf{k}' \in \text{B.Z.}} e^{i(\mathbf{k}-\mathbf{k}') \cdot \mathbf{r}_i} c_{\mathbf{k}}^\dagger c_{\mathbf{k}'}.
\end{aligned}
\tag{3.12}
$$

With nearest neighbors, we can transform the position index j in terms of the index i and a primitive unit vector $\mathbf{r}_j \to \mathbf{r}_i \pm \mathbf{a}_{x/y}$. Furthermore, one can compute the sum across the position index i to get the Kronecker delta $\delta_{\mathbf{k}\mathbf{k}'} = (1/N) \sum_i \exp(i(\mathbf{k} - \mathbf{k}') \cdot \mathbf{r}_i)$,

$$
\begin{aligned}
\hat{H}_{0,\sigma} &= -\frac{t}{N} \sum_{i}^{N} \sum_{\mathbf{k},\mathbf{k}' \in \text{B.Z.}} e^{i(\mathbf{k}-\mathbf{k}') \cdot \mathbf{r}_i} \left[e^{ik_x' a} + e^{-ik_x' a} + e^{ik_y' a} + e^{-ik_y' a} \right] c_{\mathbf{k}}^\dagger c_{\mathbf{k}'} - \mu \sum_{\mathbf{k} \in \text{B.Z.}} c_{\mathbf{k}}^\dagger c_{\mathbf{k}} \\
&= \sum_{\mathbf{k} \in \text{B.Z.}} \left(-\mu - 2t[\cos(k_x a) + \cos(k_y a)] \right) c_{\mathbf{k}}^\dagger c_{\mathbf{k}}.
\end{aligned}
\tag{3.13}
$$

The origin of the Kronecker delta is derived in Appendix A.5. Meanwhile, the resulting prefactor above is just the eigenenergy $\epsilon_{\mathbf{k}}$,

$$
\epsilon_{\mathbf{k}} = -\mu - 2t \left[\cos(k_x a) + \cos(k_y a) \right]. \tag{3.14}
$$

Using Eq. (3.14), one can perform checks for the diagonalization results to its real-space counterpart.

One can also generalize tight-binding models for different structure and length scale of electronic interactions as well as extending the Laplace operator to higher order of the Lagrange polynomial [19]. However, this is beyond the scope and interest of this thesis.

3.1.2 Peierls substitution: gauge transformation under magetic fields

In the presence of electromagnetic field, our initial Hamiltonian in Eq. (3.1) will experience a perturbation due to the fields, such that it becomes the minimal coupling Hamiltonian, where one performs a replacement of the kinetic momentum with the canonical momentum $\hbar \mathbf{k} \to \mathbf{p} - \frac{e}{c}\mathbf{A}$ [20],

$$
h(\mathbf{r}) = \frac{(\mathbf{p} - \frac{e}{c}\mathbf{A}(\mathbf{r}))^2}{2m} + \sum_{i}^{N} V(\mathbf{r} - \mathbf{r}_i), \tag{3.15}
$$

where $\mathbf{A}$ is the vector potential generating the perturbative magnetic field. From this, it is clear that there will be extra terms arising from $\mathbf{p} \cdot \mathbf{A}$ components when expanding the terms inside the parenthesis. As a consequence, our previously derived tight-binding model Hamiltonian would acquire extra terms of $\mathbf{A}$.

To fix this, Peierls propose a simple gauge transformation on the vector potential [21],

$$\mathbf{A}(\mathbf{r}) \rightarrow \mathbf{A}(\mathbf{r}) + \boldsymbol{\nabla}\Lambda. \tag{3.16}$$

It is then required that the Wannier wavefunctions are transformed so that the Hamiltonian with the new vector potential remains consistent with its matrix form [20],

$$\phi(\mathbf{r} - \mathbf{r}_i) \rightarrow \phi(\mathbf{r} - \mathbf{r}_i)e^{i\frac{e}{\hbar c}\Lambda_i(\mathbf{r})}. \tag{3.17}$$

$\Lambda_i(\mathbf{r})$ is the gauge function of the transformation for lattice site i,

$$\Lambda_i(\mathbf{r}) = \int_{\mathbf{r}_i}^{\mathbf{r}} d\mathbf{r}' \cdot \mathbf{A}(\mathbf{r}') = \int_0^1 d\lambda(\mathbf{r} - \mathbf{r}_i) \cdot \mathbf{A}(\mathbf{r}_i + \lambda(\mathbf{r} - \mathbf{r}_i)) \tag{3.18}$$

The line integral is taken as a straight line from the lattice site $\mathbf{r}_i$ to $\mathbf{r}$. This is done by parametrization of $\mathbf{r}' = \mathbf{r}_i + \lambda(\mathbf{r} - \mathbf{r}_i)$.

Now to show that the resulting dynamics is consistent in the transformation, we shall apply the Hamilton operator $\tilde{h}(\mathbf{r})$ to the transformed field operator $\tilde{\Psi}_\sigma(\mathbf{r})$[22]. Without loss of generality, we will consider $V(\mathbf{r} - \mathbf{r}_i) = 0$,

$$\begin{aligned}
\tilde{h}(\mathbf{r})\tilde{\Psi}_\sigma(\mathbf{r}) &= \frac{1}{2m}\left[-i\hbar\boldsymbol{\nabla} - \frac{e}{c}\mathbf{A}(\mathbf{r})\right]^2 \sum_i^N \tilde{\phi}(\mathbf{r} - \mathbf{r}_i)c_{i\sigma} \\
&= \frac{1}{2m}\left[-i\hbar\boldsymbol{\nabla} - \frac{e}{c}\mathbf{A}(\mathbf{r})\right]^2 \sum_i^N \phi(\mathbf{r} - \mathbf{r}_i)e^{i\frac{e}{\hbar c}\Lambda_i(\mathbf{r})}c_{i\sigma} \\
&= \sum_i^N e^{i\frac{e}{\hbar c}\Lambda_i(\mathbf{r})}\frac{1}{2m}\left[-i\hbar\boldsymbol{\nabla} - \frac{e}{c}\mathbf{A}(\mathbf{r}) + \frac{e}{c}\boldsymbol{\nabla}\Lambda_i(\mathbf{r})\right]^2 \phi(\mathbf{r} - \mathbf{r}_i)c_{i\sigma}
\end{aligned} \tag{3.19}$$

Some simplifying assumptions taken for this study is a spatially homogeneous external magnetic field $\mathbf{B}_\mathrm{a}$ as well as the locality of the Wannier wavefunctions where $\mathbf{r} \approx \mathbf{r}_i$. As explained in detail in Appendix A.6, the gradient of the gauge function can be approximated by $\boldsymbol{\nabla}\Lambda_i(\mathbf{r}) \approx \mathbf{A}(\mathbf{r})$ in the equation above.

One will finally obtain a similiar form of tight-binding Hamiltonian, with an additional complex phase on each site,

$$\tilde{h}(\mathbf{r})\tilde{\Psi}_\sigma(\mathbf{r}) = \sum_i^N e^{i\frac{e}{\hbar c}\Lambda_i(\mathbf{r})}h(\mathbf{r})\phi(\mathbf{r} - \mathbf{r}_i)c_{i\sigma}. \tag{3.20}$$

The transformation above consequently leads to the complex phase in the hopping integral,

$$\hat{H}_{0,\sigma} = -\frac{\hbar^2}{2m}\sum_{i,j}^N \int d^2\mathbf{r}\, e^{i\frac{e}{\hbar c}(\Lambda_i(\mathbf{r}) - \Lambda_j(\mathbf{r}))}\phi^*(\mathbf{r} - \mathbf{r}_i)\boldsymbol{\nabla}^2\phi(\mathbf{r} - \mathbf{r}_j)c_{i\sigma}^\dagger c_{j\sigma}. \tag{3.21}$$

However, one may notice that with an additional complex phase from the adjoint of the quantum field operator, the phase difference $\theta_{ij} = \Lambda_i - \Lambda_j$ is entirely independent of $\mathbf{r}$, and only the line integral from $\mathbf{r}_i$ to $\mathbf{r}_j$ remains,

$$\theta_{ij} = \Lambda_i(\mathbf{r}) - \Lambda_j(\mathbf{r}) = \int_{\mathbf{r}_i}^{\mathbf{r}} d\mathbf{r}' \cdot \mathbf{A}(\mathbf{r}') - \int_{\mathbf{r}_j}^{\mathbf{r}} d\mathbf{r}' \cdot \mathbf{A}(\mathbf{r}')$$
$$= \int_{\mathbf{r}_i}^{\mathbf{r}_j} d\mathbf{r}' \cdot \mathbf{A}(\mathbf{r}') \tag{3.22}$$

Therefore the hopping integral under magnetic field is transformed to

$$t_{ij} \rightarrow t_{ij} e^{i\frac{e}{\hbar c}\theta_{ij}}. \tag{3.23}$$

Following Stoke's theorem, taking a closed path around the unit cell in the system corresponds to smallest possible magnetic field,

$$\oint_{\text{unit cell}} d\mathbf{r}' \cdot \mathbf{A}(\mathbf{r}') = \int d^2\mathbf{r}' \hat{\mathbf{n}} \cdot (\boldsymbol{\nabla} \times \mathbf{A})$$
$$= \int d^2\mathbf{r}' \hat{\mathbf{n}} \cdot \mathbf{B} \tag{3.24}$$
$$= \Phi.$$

Φ is the phase acquired when going around a unit cell, defined as the flux per plaquette. As one may notice, relative to the complex phase, its physical dimension is comparable to the flux quantum $\Phi_0 = \frac{hc}{2e}$. Therefore, it is also useful to write the magnetic field contribution α in terms of Φ_0 where

$$\alpha = \frac{\Phi}{2\Phi_0}. \tag{3.25}$$

From Hofstadter's explicit calculation using the momentum-space, it is also shown that the applied field α has to be rational, with $\alpha = \frac{p}{q}$ where $p, q \in \mathbb{Z}$ [23].

Throughout this study, we will use the Landau gauge, $\mathbf{A}(\mathbf{r}) = -By\mathbf{e}_{\text{x}}$ as the generating vector potential. By this choice of gauge, the hopping integral along the x-direction $t_{x\pm a}$ carries a complex phase, while hopping integral along y-direction $t_{y\pm a}$ carries no complex phase as shown below,

$$t_{ij,\text{x}\pm} = t_{ij} e^{\pm i\frac{\pi}{\Phi_0}By}$$
$$t_{ij,\text{y}\pm} = t_{ij} \tag{3.26}$$

3.1.3 Magnetic vector potential in boundary hoppings

In the beginning of this chapter, we have used Born-von-Karman boundary conditions to impose a translational invariance across lattice lengths with $e^{i\mathbf{k}\cdot L_i\mathbf{a}_i}\Psi(\mathbf{r}) = \Psi(\mathbf{r} + L_i\mathbf{a}_i)$. This, however, does not hold for metals subject to magnetic fields. Despite a uniform magnetic field, the vector potential is linear in y.

To take into account this effect, we need to conceptualize hopping across boundaries of the magnetic unit cell (MUC). A magnetic unit cell is defined here as the cell in our tight-binding system that has translational symmetry also in presence of a
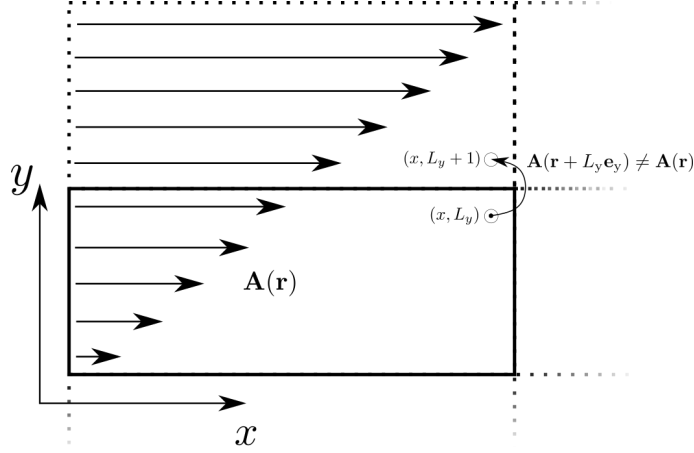
Figure 3.1: Vector potential increases linearly with y in the Landau gauge, breaking translational invariance.

magnetic field. Note that this cell does not necessarily have to be the smallest possible cell to represent that symmetry. In this thesis, the magnetic unit cell is conveniently chosen to be of the size of the lattice, $N = L_x L_y$.

As an electron jump across boundaries, the hopping integral is usually mapped back periodically in a Hamiltonian (i.e coordinate $(x, L_y) \leftrightarrow (x, 1)$). When there is magnetic field in the system, lattice sites across boundary are subject to vector potential $\mathbf{A}(\mathbf{r} \pm L_y \mathbf{e}_y)$ rather than $\mathbf{A}(\mathbf{r})$ (see Fig. 3.1). This is not considered by a phaseless hopping integral t_{ij} along the magnetic unit cell boundaries.

To resolve this issue while maintaining periodic hopping in our Hamiltonian, one can use a gauge transformation along the boundaries [22],

$$\mathbf{A}(\mathbf{r}) \to \mathbf{A}(\mathbf{r} + L_i \mathbf{e}_i) = \mathbf{A}(\mathbf{r}) + \boldsymbol{\nabla} \Lambda_i, \quad i = \mathrm{x}, \mathrm{y}. \tag{3.27}$$

One can calculate explicitly the scalar field for hoppings in the x- and y-direction using our Landau gauge.

Since the vector potential is independent of x, we can immediately conclude that the scalar field is constant in the x-direction,

$$\mathbf{A}(\mathbf{r} \pm L_{\mathrm{x}} \mathbf{e}_{\mathrm{x}}) = -By\mathbf{e}_{\mathrm{x}} = \mathbf{A}(\mathbf{r})$$
$$\implies \Lambda_{\mathrm{x}} = c, \text{ where } c \in \mathbb{R} \implies \text{W.L.O.G. } \Lambda_{\mathrm{x}} = 0. \tag{3.28}$$

On the other hand, the gauge transformation has a non-trivial scalar field in the y-direction,

$$\mathbf{A}(\mathbf{r} \pm L_{\mathrm{y}} \mathbf{e}_{\mathrm{y}}) = -B(y \pm L_{\mathrm{y}})\mathbf{e}_{\mathrm{x}}$$
$$\implies \boldsymbol{\nabla} \Lambda_i = \mp BL_{\mathrm{y}} \mathbf{e}_{\mathrm{x}} \implies \Lambda_{\mathrm{y}} = \mp BL_{\mathrm{y}} x. \tag{3.29}$$

Similar to the previous section, the Wannier wavefunction corresponding to coordinate $y + L_y$ will also be transformed accordingly,

$$\phi(\mathbf{r} - \mathbf{r}_i) \to \phi(\mathbf{r} - \mathbf{r}_i) e^{i\frac{e}{\hbar c}\Lambda_{\mathrm{y}}}. \tag{3.30}$$

Computing the hopping integral analagous to Eq. (3.21), one will also obtain a transformation in the hopping integral,

$$t_{ij,\mathrm{y},\mathrm{boundary}\pm} = t_{ij} e^{\mp i\frac{\pi}{\Phi_0} BL_{\mathrm{y}} x}$$
$$t_{ij,\mathrm{x},\mathrm{boundary}\pm} = t_{ij}. \tag{3.31}$$

With this, we can maintain the periodic hoppings constructed in the tight-binding Hamiltonian. A more rigorous approach can also be done for arbitrary vector potentials using the magnetic translation operator. From this, one can then use the supercell method to optimize calculation of many Brillioun zones [24].

3.1.4 Hofstadter's butterfly: tight-binding energy spectrum in a magnetic field

Summarizing the two previous discussions, applying an external magnetic field, we obtained two different kinds of complex phases in the hopping integral. The first is the Peierls' substitution in Eq. (3.26) to maintain our structure of the Hamiltonian. Additionally we include another transformation through Eq. (3.31) to account for the change in vector potentials in hoppings across the magnetic unit cell boundary.

If the Peierls' subsititution is applied correctly, one can observe the forming of bands in the energy spectrum of the system, following a fractal pattern called the Hofstadter butterfly. Hofstadter analytically found this pattern by solving Schrödinger's equation from non-interacting electrons in magnetic fields using Harper's equation [23]. To check our implementation of the Peierls substitution, we reproduce the pattern in Fig. 3.2 by numerically calculating the eigenvalues of the real space tight binding Hamiltonian.

As shown in the Hofstadter butterfly, for some rational value $\alpha = \frac{p}{q}$ the spectrum forms exactly q bands. Due to spin-invariance of the eigenenergy of the tight binding model, one will also observe that the spectrum for $+\alpha$ is the same as $-\alpha$, and that the butterfly follows a periodic pattern along integer multiples.
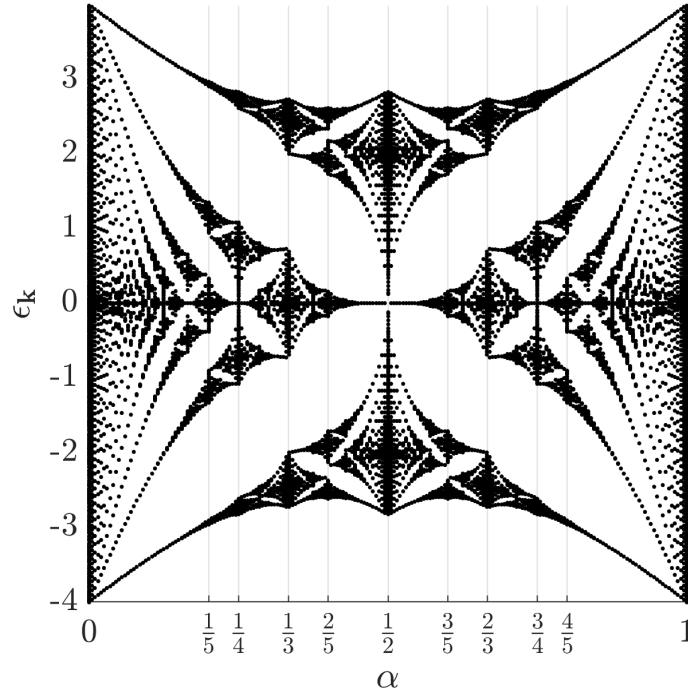
Figure 3.2: Hofstadter butterfly, obtained from a system with 100×25 lattice points, subject to magnetic field parametrized by $\alpha = \frac{\Phi}{2\Phi_0}$.

On the other hand, energy spectrum of the Hofstadter butterfly may still be observed without employing the boundary hoppings in Eq. (3.31). This follows as transforming the boundary hoppings corresponds to a uniform complex phase shift in the eigenvectors corresponding to the same eigenenergy [24].

3.2 Conventional superconductivity in real space formulation

In this study, we will consider s-wave superconductivity found in most conventional superconductors. In conventional superconductors, a phonon-driven mechanism causes the attractive correlations between electrons. Furthermore, the s-wave symmetry involves singlet-state pairings, where opposite spin electrons form a Cooper pair. We take a semi-classical approach by Altland's "Condensed Matter Field Theory" to explain this interactions [18].

Consider electrons moving through a ionic lattice. The motion of an electron will then cause a distortion of the ions from the equilibrium position. For an electron, the time it takes for it to traverse through the ion is at the time scale that corresponds to the Fermi energy $\sim E_F^{-1}$. On the other hand, the time an ion needs to relax back to its equilibrium position is at the scale of the Debye frequency $\sim \omega_D^{-1} \gg E_F^{-1}$.

As shown in Fig. 3.3, such lattice distortions create an effective attractive interaction between electrons. The two fermions create an electron-electron bound state known
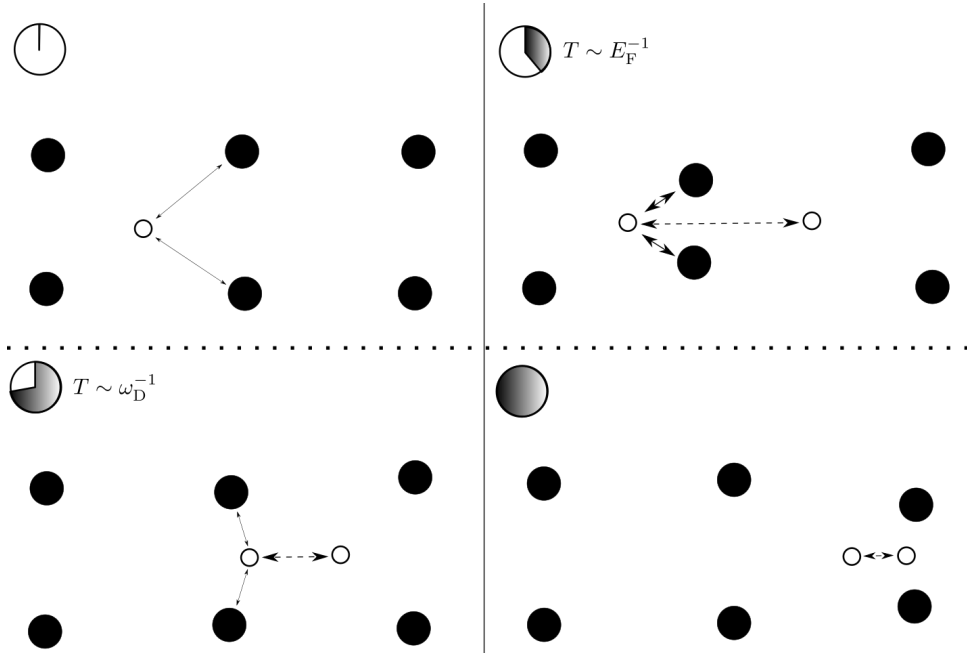
Figure 3.3: Ionic lattice (black dots) distortion due to Coulomb interaction (solid arrow) by an electron (white dots) at different time scales. The lag between the time needed to traverse through the electron, with the relaxation of the ion to equilibrium, cause an effective attractive interaction (dotted arrow) between electrons. Adapted from Ref. [18].

as Cooper pair. Sum of the electron spins forms integer total spins, which mimic the behaviour of bosonic particles.

In s-wave superconductivity, Cooper pairs are formed through singlet states, such that electron pairs are restricted to $|\uparrow\downarrow\rangle$, $|\downarrow\uparrow\rangle$ states. Furthermore, within the Fermi level it becomes energetically favourable to form pairs with a total momentum $\mathbf{Q} = \mathbf{k} + (-\mathbf{k}) = 0$, reducing the total energy in the ground state. This then leads to formation of a bound pair of time-reversed states $|\mathbf{k}\uparrow, -\mathbf{k}\downarrow\rangle$.

In the next section we will start from a pairing interaction that leads to s-wave superconductivity. By means of the mean-field decoupling of the interaction, rewriting the Hamiltonian using a basis with Nambu spinors, we finally obtain the eigenstates within the Bogoliubov de Gennes formalism. This procedure is a variant of the BCS theory.

3.2.1 Mean-field decoupling for arbitrary products

The phonon mechanism for superconductivity leads to a Hamiltonian that exhibits an interaction term. To simplify this, we can use mean-field approximation to treat the interactions of each particle as an interaction between an individual particle with an average field of the rest of the particles in a system. To discuss the general steps of the mean-field approach, we present the decoupling for a generic Hamiltonian as discussed by Bruus and Flensberg [13].

Suppose we have a Hamiltonian of coupled interactions formed by products of two operators,

$$H_{AB} = AB. \tag{3.32}$$

We can rewrite each operator as its mean and fluctuations δA and δB,

$$\begin{aligned} A &= \langle A \rangle + \delta A \\ B &= \langle B \rangle + \delta B. \end{aligned} \tag{3.33}$$

Inserting Eq. (3.33) to the Hamiltonian, we have

$$H_{AB} = \langle A \rangle \langle B \rangle + \langle A \rangle \delta B + \langle B \rangle \delta A + \delta A \delta B. \tag{3.34}$$

Assuming that due to some physical arguments, the operator A and B deviate little from their average values, $\langle A \rangle$ and $\langle B \rangle$, we can argue that the fluctuations δA and δB are small relative to its mean. With this, the final term in the Hamiltonian above can be removed, since it is quadratic in fluctuations. Furthermore, we shall expand the linear fluctuations back to its mean field form, by solving Eq. (3.33) for δA and δB, leading to the mean-field Hamiltonian,

$$H_{AB,\text{MF}} = \langle A \rangle B + \langle B \rangle A - \langle A \rangle \langle B \rangle. \tag{3.35}$$

3.2.2 Electronic interactions and the SC order parameter

So far, we have only included the non-interacting tight-binding model. To theoretically incorporate the s-wave superconductivity, the aforementioned interactions between electrons have to be taken into account. Recall the interaction Hamiltonian,

$$\hat{V}_{\text{ee},\sigma\sigma'} = \frac{1}{2} \iint d^2\mathbf{r}d^2\mathbf{r}' V_{\text{ee}}(\mathbf{r},\mathbf{r}')\Psi_\sigma^\dagger(\mathbf{r})\Psi_{\sigma'}^\dagger(\mathbf{r}')\Psi_{\sigma'}(\mathbf{r}')\Psi_\sigma(\mathbf{r}). \tag{3.36}$$

Similar to the previous section, we will use the Wannier basis in Eq. (3.4) to obtain,

$$\hat{V}_{\text{ee},\sigma\sigma'} = \frac{1}{2}\sum_{i,j,k,l}^N V_{\text{ijkl}}c_{i\sigma}^\dagger c_{j\sigma'}^\dagger c_{k\sigma'}c_{l\sigma},$$

$$V_{\text{ijkl}} = \iint d^2\mathbf{r}d^2\mathbf{r}' V_{\text{ee}}(\mathbf{r},\mathbf{r}')\phi^*(\mathbf{r}-\mathbf{r}_i)\phi^*(\mathbf{r}'-\mathbf{r}_j)\phi(\mathbf{r}'-\mathbf{r}_k)\phi(\mathbf{r}-\mathbf{r}_l). \tag{3.37}$$

From the phonon-driven pairing mechanism we assume a uniform attractive interaction $V < 0$ across all sites. Which gives us the attractive Hubbard model [18],

$$\hat{V}_{\text{ee},\uparrow\downarrow} = \hat{V}_{\text{ee},\downarrow\uparrow} = \frac{V}{2}\sum_i^N c_{i\uparrow}^\dagger c_{i\downarrow}^\dagger c_{i\downarrow}c_{i\uparrow}. \tag{3.38}$$

With the four operators, calculating the overall correlated effects of the 2-particle interactions can be done through exact diagonalization. However, the Hilbert space for such multi-particle systems grows exponentially and diagonalization becomes computationally impossible to do.

In s-wave superconductors, we have a finite expectation of the operator $\langle c_{i\downarrow}c_{i\uparrow}\rangle \neq 0$, which represents the forming of Cooper pairs from opposite spins. Performing mean-field approximation in the interaction Hamiltonian, Eq. (3.38) then gets replaced by

$$\hat{V}_{\text{ee},\uparrow\downarrow}^{\text{MF}} = \hat{V}_{\text{ee},\downarrow\uparrow}^{\text{MF}} = \frac{V}{2}\sum_i^N \left(\langle c_{i\uparrow}^\dagger c_{i\downarrow}^\dagger\rangle c_{i\downarrow}c_{i\uparrow} + \langle c_{i\downarrow}c_{i\uparrow}\rangle c_{i\uparrow}^\dagger c_{i\downarrow}^\dagger - \langle c_{i\uparrow}^\dagger c_{i\downarrow}^\dagger\rangle \langle c_{i\downarrow}c_{i\uparrow}\rangle\right). \tag{3.39}$$

The expectation value $\langle c_{i\uparrow}^\dagger c_{i\downarrow}^\dagger\rangle$ can then be calculated self-consistently, which will be discussed in later chapters. Taking into account terms from all spin combinations, the interacting Hamiltonian is,

$$\hat{V}_{\text{ee}}^{\text{MF}} = \sum_i^N \left(\Delta_i^* c_{i\downarrow}c_{i\uparrow} + \Delta_i c_{i\uparrow}^\dagger c_{i\downarrow}^\dagger - \frac{|\Delta_i|^2}{V}\right). \tag{3.40}$$

We have parametrized the average field of the Cooper pairs as the superconducting order (gap) parameter,

$$\Delta_i = V\langle c_{i\downarrow}c_{i\uparrow}\rangle. \tag{3.41}$$

As one can see, we have transformed our 2-particle operator into a single-particle operator which can be written in a matrix form. This will be useful in the following discussions when we try solve for the average-fields.

3.2.3 Nambu spinor

Combining the interaction and tight-binding Hamiltonian, we obtain the mean-field BCS Hamiltonian,

$$\hat{H}_{\text{BCS}}^{\text{MF}} = -\sum_{\langle i,j\rangle,\sigma}^N t_{ij}c_{i\sigma}^\dagger c_{j\sigma} - \mu\sum_{i,\sigma}^N c_{i\sigma}^\dagger c_{i\sigma} + \sum_i^N \left(\Delta_i^* c_{i\downarrow}c_{i\uparrow} + \Delta_i c_{i\uparrow}^\dagger c_{i\downarrow}^\dagger\right). \tag{3.42}$$

In the Hamiltonian above, the non-interacting term $\sim |\Delta|^2$ has been dropped[1]. Note that the hopping integral t_{ij} is defined by Eq. (3.26) and (3.31) if a magnetic field is present.

Recall that the tight binding Hamiltonian can be written in matrix form in terms of products of the matrix $H_{0,\sigma}$ in Eq. (3.11), and the creation/annihilation operators $\mathbf{c}^\dagger_\sigma = (c^\dagger_{1\sigma}, c^\dagger_{2\sigma}, ..c^\dagger_{N\sigma})$ and $\mathbf{c}_\sigma = (c_{1\sigma}, c_{2\sigma}, ..c_{N\sigma})^{\mathrm{T}}$. Analogously one can also rewrite the mean-field BCS Hamiltonian,

$$\hat{H}^{\mathrm{MF}}_{\mathrm{BCS}} = \sum_\sigma \mathbf{c}^\dagger_\sigma H_{0,\sigma} \mathbf{c}_\sigma + \mathbf{c}^\dagger_\uparrow \Delta \mathbf{c}^{\dagger\mathrm{T}}_\downarrow + \mathbf{c}^{\mathrm{T}}_\downarrow \Delta^* \mathbf{c}_\uparrow. \tag{3.43}$$

The gap matrix Δ is just the real-space gap parameters set along a diagonal matrix, $\mathrm{diag}(\Delta_1, \Delta_2, \ldots, \Delta_{\mathrm{N}})$.

We shall now introduce the Nambu spinor [18],

$$\boldsymbol{\Psi}^\dagger = \begin{pmatrix} \mathbf{c}^\dagger_\uparrow & \mathbf{c}^{\mathrm{T}}_\downarrow \end{pmatrix},$$
$$\boldsymbol{\Psi} = \begin{pmatrix} \mathbf{c}_\uparrow \\ \mathbf{c}^{\dagger\mathrm{T}}_\downarrow \end{pmatrix}. \tag{3.44}$$

With the spinors, we can now form a $2N \times 2N$ matrix of the mean-field BCS Hamiltonian,

$$\hat{H}^{\mathrm{MF}}_{\mathrm{BCS}} = \boldsymbol{\Psi}^\dagger H^{\mathrm{MF}}_{\mathrm{BCS}} \boldsymbol{\Psi}$$
$$H^{\mathrm{MF}}_{\mathrm{BCS}} = \left(\begin{array}{c|c} H_{0,\uparrow} & \Delta \\ \hline \Delta^\dagger & -H^*_{0,\downarrow} \end{array} \right). \tag{3.45}$$

The bottom right block of the matrix is obtained by flipping the order of the annihilation and creation operator $c_{i\downarrow} c^\dagger_{j\downarrow} \to -c^\dagger_{j\downarrow} c_{i\downarrow}$ and using the relation that $t^*_{ij} = t_{ji}$. The latter can be shown by transforming Eq. (3.10),

$$\begin{aligned}
t^*_{ij} &= t \int d^2\mathbf{r}\, \phi(\mathbf{r} - \mathbf{r}_i) \boldsymbol{\nabla}^2 \phi^*(\mathbf{r} - \mathbf{r}_j) \\
&= t \int d^2\mathbf{r}\, (\boldsymbol{\nabla} \cdot \left[\phi_i(\mathbf{r}) \boldsymbol{\nabla} \phi^*_j(\mathbf{r}) - \phi^*_j(\mathbf{r}) \boldsymbol{\nabla} \phi_i(\mathbf{r}) \right] + \phi^*_j(\mathbf{r}) \boldsymbol{\nabla}^2 \phi_i(\mathbf{r})) \\
&= t \oint_{|\mathbf{r}| \to \infty} dl(\hat{\mathbf{n}} \cdot [\phi_i(\mathbf{r}) \boldsymbol{\nabla} \phi^*_j(\mathbf{r}) - \phi^*_j(\mathbf{r}) \boldsymbol{\nabla} \phi_i(\mathbf{r})]) + t \int d^2\mathbf{r}\, \phi^*_j(\mathbf{r}) \boldsymbol{\nabla}^2 \phi_i(\mathbf{r}) \\
&= t_{ji}.
\end{aligned} \tag{3.46}$$

3.2.4 Bogoliubov-de Gennes equation

It turns out that the eigenstates and eigenenergies of the BCS Hamiltonian can be obtained from a diagonalization of the BCS Hamiltonian; this is derived from the Bogoliubov-de Gennes equations.

---

[1]The constant term is generally accounted for in diagonalization through the mean-field interaction term $\Delta^*_i c_{i\downarrow} c_{i\uparrow} + $ h.c.. However, it is important to remember that it is still crucial to take the constant term into account when comparing absolute internal energies $\langle H \rangle$ between systems.

To obtain the Bogoliubov-de Gennes equation, one starts by a general Bogoliubov transformation [25],

$$c_{i\sigma} = \sum_j (u_{ij\sigma}\gamma_{j\sigma} + v_{ij\sigma}^*\gamma_{j\bar{\sigma}}^\dagger). \tag{3.47}$$

It is then clear that following the fermionic anti-commutation relations in $\gamma_{i\sigma}$ must be similar for the anti-commutation relation in the original basis $c_{i\sigma}$ to hold,

$$
\begin{aligned}
\{\gamma_{i\sigma}^\dagger, \gamma_{\mathrm{j}\sigma'}\} &= \delta_{ij}\delta_{\sigma\sigma'}, \\
\{\gamma_{i\sigma}, \gamma_{\mathrm{j}\sigma'}\} &= 0, \\
\{\gamma_{i\sigma}^\dagger, \gamma_{\mathrm{j}\sigma'}^\dagger\} &= 0.
\end{aligned}
\tag{3.48}
$$

Under this transformation, we impose a diagonal Hamiltonian in the annihilation and creation operator $\gamma_{i\sigma}$ and $\gamma_{i\sigma}^\dagger$,

$$\hat{H}_{\mathrm{BCS}}^{\mathrm{MF}} = \sum_{i\sigma} E_{i\sigma}\gamma_{i\sigma}^\dagger\gamma_{i\sigma}. \tag{3.49}$$

Now we shall evaluate commutation relation of each creation operators with the BCS Hamiltonian, by using $[AB, C] = A\{B, C\} - \{A, C\}B$.

In the γ_i-operator, we have,

$$\left[\hat{H}_{\mathrm{BCS}}^{\mathrm{MF}}, \gamma_{i\sigma}\right] = \sum_{j\sigma}^N E_{j\sigma}(\gamma_{j\sigma}^\dagger\{\gamma_{j\sigma}, \gamma_{i\sigma}\} - \{\gamma_{j\sigma}^\dagger, \gamma_{i\sigma}\}\gamma_{j\sigma}) = -E_{i\sigma}\gamma_{i\sigma},$$

$$\left[\hat{H}_{\mathrm{BCS}}^{\mathrm{MF}}, \gamma_{i\sigma}^\dagger\right] = E_{i\sigma}\gamma_{i\sigma}^\dagger. \tag{3.50}$$

On the other hand, in the old c_i-operator, we have,

$$\left[\hat{H}_{\mathrm{BCS}}^{\mathrm{MF}}, c_{i\uparrow}\right] = -\sum_j^N (H_{0\uparrow})_{ji}c_{i\uparrow} - (\Delta)_{ii}c_{i\downarrow}^\dagger,$$

$$\left[\hat{H}_{\mathrm{BCS}}^{\mathrm{MF}}, c_{i\downarrow}\right] = -\sum_j^N (H_{0\downarrow})_{ji}c_{i\downarrow} + (\Delta)_{ii}c_{i\uparrow}^\dagger, \tag{3.51}$$

where we have considered the pairing term to be diagonal.

By inserting the Bogoliubov transformations in Eq. (3.51), we can compare the terms of both side of the equations within each operator $\gamma_{i\sigma}$ and $\gamma_{i\sigma}^\dagger$ to obtain a system of equations,

$$E_{j\uparrow}u_{ij\uparrow} = \sum_k^N (H_{0\uparrow})_{ki}u_{ij\uparrow} + (\Delta)_{ii}v_{ij\downarrow}$$

$$E_{j\uparrow}v_{ij\downarrow} = (\Delta)_{ii}u_{ij\uparrow} - \sum_k^N (H_{0\downarrow})_{ki}^*v_{ij\downarrow}$$

$$E_{j\downarrow}v_{ij\uparrow} = -\sum_k^N (H_{0\uparrow})_{ki}^*v_{ij\uparrow} - (\Delta)_{ii}^*u_{ij\downarrow}$$

$$E_{j\downarrow}u_{ij\downarrow} = -(\Delta)_{ii}v_{ij\uparrow} + \sum_k^N (H_{0\downarrow})_{ki}u_{ij\downarrow}. \tag{3.52}$$

We have now found our eigenvectors in terms of the coefficients of the Bogoliubov transformation, leading to the matrix form of the Bogoliubov equations,

$$
\begin{aligned}
H_{\text{BCS}}^{\text{MF}} \begin{pmatrix} \mathbf{u}_\uparrow \\ \mathbf{v}_\downarrow \end{pmatrix}^j &= \left(\begin{array}{c|c} H_{0\uparrow} & \Delta \\ \hline \Delta^* & -H_{0\downarrow}{}^* \end{array} \right) \begin{pmatrix} \mathbf{u}_\uparrow \\ \mathbf{v}_\downarrow \end{pmatrix}^j = E_{j\uparrow} \begin{pmatrix} \mathbf{u}_\uparrow \\ \mathbf{v}_\downarrow \end{pmatrix}^j \\
-H_{\text{BCS}}^{\text{MF}\,*} \begin{pmatrix} \mathbf{v}_\uparrow \\ \mathbf{u}_\downarrow \end{pmatrix}^{j'} &= \left(\begin{array}{c|c} -H_{0\uparrow}{}^* & -\Delta^* \\ \hline -\Delta & H_{0\downarrow} \end{array} \right) \begin{pmatrix} \mathbf{v}_\uparrow \\ \mathbf{u}_\downarrow \end{pmatrix}^{j'} = E_{j'\downarrow} \begin{pmatrix} \mathbf{v}_\uparrow \\ \mathbf{u}_\downarrow \end{pmatrix}^{j'} .
\end{aligned}
\tag{3.53}
$$

From above, one can see that the $E_{j\uparrow}$ and $E_{j\downarrow}$ are separated by a transformation on the leading Hamiltonian. We can derive from this, the relations between the two eigenenergies.

We start by evaluating the conjugated spin-down Hamiltonian,

$$
\left(-H_{\text{BCS}}^{\text{MF}\,*} \begin{pmatrix} \mathbf{v}_\uparrow \\ \mathbf{u}_\downarrow \end{pmatrix}^{j'} \right)^* = E_{j'\downarrow} \begin{pmatrix} \mathbf{v}_\uparrow^* \\ \mathbf{u}_\downarrow^* \end{pmatrix}^{j'} .
\tag{3.54}
$$

Since our conjugated the spin-down Hamiltonian leads to an eigenenergy, one can deduce that the conjugated spin-down eigenvector $(\mathbf{v}_\uparrow^*, \mathbf{u}_\downarrow^*)_{j'}^{\text{T}}$ is also an eigenvector of the spin-up Hamiltonian $H_{\text{BCS}}^{\text{MF}}$. Therefore, we can also write it as the spin-up eigenvector $(\mathbf{u}_\uparrow, \mathbf{v}_\downarrow)_{j'}^{\text{T}}$,

$$
\left(-H_{\text{BCS}}^{\text{MF}\,*} \begin{pmatrix} \mathbf{v}_\uparrow \\ \mathbf{u}_\downarrow \end{pmatrix}^{j'} \right)^* = -H_{\text{BCS}}^{\text{MF}} \begin{pmatrix} \mathbf{u}_\uparrow \\ \mathbf{v}_\downarrow \end{pmatrix}^{j'} = -E_{j'\uparrow} \begin{pmatrix} \mathbf{u}_\uparrow \\ \mathbf{v}_\downarrow \end{pmatrix}^{j'} .
\tag{3.55}
$$

From the above, one can see that it is sufficient to diagonalize only one matrix from the Bogoliubov equations in Eq. (3.53). By keeping in mind of the transformation in the eigenvectors between $\uparrow$ and $\downarrow$ spins, the spin can then be suppressed to a single spin. This will be useful for calculations physical parameters in the coming sections.

We can now derive the gap equation in the γ_i-operator by inserting the Bogoliubov transformation in the definition of the superconducting order parameter in Eq. (3.41),

$$
\begin{aligned}
\Delta_i =& V \sum_{j,k}^N \Big(u_{ij\downarrow} u_{ik\uparrow} \underbrace{\langle \gamma_{j\downarrow} \gamma_{k\uparrow} \rangle}_{0} + v_{ij\downarrow}^* u_{ik\uparrow} \underbrace{\langle \gamma_{j\uparrow}^\dagger \gamma_{k\uparrow} \rangle}_{\delta_{jk} f(E_{j\uparrow})} \\
& + u_{ij\downarrow} v_{ik\uparrow}^* \underbrace{\langle \gamma_{j\downarrow} \gamma_{k\downarrow}^\dagger \rangle}_{\delta_{jk}(1 - f(E_{j\downarrow}))} + v_{ij\downarrow}^* v_{ik\uparrow}^* \underbrace{\langle \gamma_{j\uparrow}^\dagger \gamma_{k\downarrow}^\dagger \rangle}_{0} \Big) \\
=& V \sum_j^N \left[v_{ij\downarrow}^* u_{ij\uparrow} f(E_{j\uparrow}) + u_{ij\downarrow} v_{ij\uparrow}^* (1 - f(E_{j\downarrow})) \right] .
\end{aligned}
\tag{3.56}
$$

In the equation above, we evaluate the expectation values in the basis of the gamma operators where the Hamiltonian is diagonal, Eq. (3.49). Therefore, two expectation values vanish, and the others are just given by the Fermi distribution $f(E)$ according to Eq. (1.9).

We know from Eq. (3.54) and (3.55), there is an equivalence in the eigenenergies $E_{j'\downarrow} = -E_{j'\uparrow}$ by invoking the eigenvector transformation $(\mathbf{v}_\uparrow^*, \mathbf{u}_\downarrow^*)_{j'}^{\text{T}} \leftrightarrow (\mathbf{u}_\uparrow, \mathbf{v}_\downarrow)_{j'}^{\text{T}}$.

Hence we can change the second term in the gap equation to $-E_{j'\uparrow}$ by transforming $u_{ij\downarrow}v_{ij\uparrow}^* \rightarrow v_{ij'\downarrow}^* u_{ij'\uparrow}$. This allows us to suppress the spin index, where u_{ij} and v_{ij} are coefficients of the i-th row and $i + N$-th row of the eigenvector respectively,

$$
\begin{aligned}
\Delta_i =& V \left\{ \sum_j^N v_{ij\downarrow}^* u_{ij\uparrow} f(E_{j\uparrow}) + \sum_j^N {}' v_{ij\downarrow}^* u_{ij\uparrow} \left[1 - f(-E_{j\uparrow}) \right] \right\} \\
=& V \left\{ \sum_j^N v_{ij\downarrow}^* u_{ij\uparrow} f(E_{j\uparrow}) + \sum_j^N {}' v_{ij\downarrow}^* u_{ij\uparrow} f(E_{j\uparrow}) \right\} \\
=& V \sum_j^N v_{ij}^* u_{ij} f(E_j).
\end{aligned}
\tag{3.57}
$$

In the calculation above, $\sum$ and $\sum'$ were each sums over half of the eigenvalue. Therefore, the final result is just the total some of the entire eigenvalues.

Similarly, the electronic number density can also be found,

$$
\langle N \rangle = \sum_{i,j}^N \left[|u_{ij}|^2 f(E_j) + |v_{ij}|^2 (1 - f(E_j)) \right].
\tag{3.58}
$$

3.2.5 Gap parameter self-consistent fixed-point iteration

As mentioned earlier, the mean-field approximation requires us to solve the gap parameter self-consistently. Therefore, an algorithm based on the fixed-point iteration method is constructed as shown in the following [26],

---

Algorithm 1: Δ_i self-consistency iterative method

Result: Self-consistent gap parameters $\mathbf{\Delta}_{\text{new}}$ and chemical potential μ for a
         target density n_{target}.

1. Determine mixing constants α and β;

2. Guess value of gap parameters $\mathbf{\Delta}_{\text{old}}$ and chemical potential μ;

3. **while** $\|\mathbf{\Delta}_{\text{old}} - \mathbf{\Delta}_{\text{new}}\|_1 / \|\mathbf{\Delta}_{\text{new}}\|_1 > \epsilon_{\text{diff}}$ *and* $\max(\{\Delta_{\text{new,i}}\}) > \epsilon_{\text{max}}$ **do**

    Construct matrix $H_{\text{BCS}}^{\text{MF}}(\mathbf{\Delta}_{\text{old}}, \mu)$;

    Diagonalize $H_{\text{BCS}}^{\text{MF}}$ to obtain eigenvector $(\mathbf{u}, \mathbf{v})^{\text{T}}$ and eigenenergy $(\{E_i\})$;

    Calculate $n = \langle N \rangle / N$ [according to Eq. (3.58)];

    Update $\mu = \mu + \beta \frac{n_{\text{target}} - n}{n_{\text{target}}}$;

    Calculate $(\mathbf{\Delta}_{\text{new}})_i = \Delta_i$ [according to Eq. (3.57)];

    Update $\mathbf{\Delta}_{\text{old}} = \mathbf{\Delta}_{\text{old}} \alpha + \mathbf{\Delta}_{\text{new}} (1 - \alpha)$;

end

4. Break iteration;

In this algorithm, the fixed-point iteration is modified with a mixing constant $\alpha, \beta \in (0, 1)$ to ensure that the convergence of the gap parameter is stable.

The convergence criterion ϵ_{diff} is given to be the 1-norm of the gap parameter vector $\boldsymbol{\Delta}$ representing the N possible different gap parameter on each site. Since numerical precision may become an issue when superconductivity vanishes, an addition criterion ϵ_{max} is given to stop the iteration once the gap reaches a value relatively close to zero.

For homogenous gap parameter, it is sufficient to set $\epsilon_{\text{diff}} \approx 10^{-4}$ and $\epsilon_{\text{max}} \approx 10^{-8}$, since the there will be negligible change throughout the entire vector $\boldsymbol{\Delta}$ for every iteration. However, it is important to consider a lower tolerance in ϵ_{diff} to achieve convergence in the vortex-state as we will discuss in the upcoming chapter.

3.2.6   BCS theory in momentum-space

So far, we have treated the BCS theory in real-space, which becomes useful when one would like to treat an inhomogeneous gap parameter, including superconductors under magnetic fields.

In the momentum-space, one can analogously develop the BCS theory. Including the interaction term in momentum-space, our BCS Hamiltonian for s-wave superconductors is written as [13],

$$\hat{H}_{\text{BCS}}^{\text{MF}} = \sum_{\mathbf{k}\sigma} \epsilon_{\mathbf{k}} c_{\mathbf{k}\sigma}^{\dagger} c_{\mathbf{k}\sigma} + \sum_{\mathbf{k}} \Delta c_{\mathbf{k}\uparrow}^{\dagger} c_{-\mathbf{k}\downarrow}^{\dagger} + \sum_{\mathbf{k}} \Delta^{*} c_{-\mathbf{k}\downarrow} c_{\mathbf{k}\uparrow}. \tag{3.59}$$

The BCS Hamiltonian in this case, sums over $\mathbf{k}$ in the Brillouin Zone. The momentum-space gap parameter is then,

$$\Delta = V \sum_{\mathbf{k}} \langle c_{\mathbf{k}\uparrow}^{\dagger} c_{-\mathbf{k}\downarrow}^{\dagger} \rangle. \tag{3.60}$$

Under the momentum-space Nambu spinor $\boldsymbol{\Psi}_{\mathbf{k}} = (c_{\mathbf{k}\uparrow}^{\dagger} \ c_{-\mathbf{k}\downarrow})$, the Hamiltonian can be written under the matrix form,

$$\hat{H}_{\text{BCS}}^{\text{MF}} = \sum_{\mathbf{k}} \begin{pmatrix} c_{\mathbf{k}\uparrow}^{\dagger} & c_{-\mathbf{k}\downarrow} \end{pmatrix} \begin{pmatrix} \epsilon_{\mathbf{k}} & \Delta \\ \Delta^{*} & -\epsilon_{\mathbf{k}} \end{pmatrix} \begin{pmatrix} c_{\mathbf{k}\uparrow} \\ c_{-\mathbf{k}\downarrow}^{\dagger} \end{pmatrix} = \sum_{\mathbf{k}} \boldsymbol{\Psi}_{\mathbf{k}} H_{\mathbf{k}} \boldsymbol{\Psi}_{\mathbf{k}}^{\dagger}. \tag{3.61}$$

Diagonalization is obtained by a simpler Bogoliubov transformation [15],

$$\begin{pmatrix} c_{\mathbf{k}\uparrow} \\ c_{-\mathbf{k}\downarrow}^{\dagger} \end{pmatrix} = \begin{pmatrix} u_{\mathbf{k}} & v_{\mathbf{k}}^{*} \\ -v_{\mathbf{k}} & u_{\mathbf{k}}^{*} \end{pmatrix} \begin{pmatrix} \gamma_{\mathbf{k}\uparrow} \\ \gamma_{-\mathbf{k}\downarrow}^{\dagger} \end{pmatrix}. \tag{3.62}$$

By parametrizing $u_{\mathbf{k}}$ and $v_{\mathbf{k}}$ as a rotational transformation, one can solve the coefficients of the transformation,

$$\begin{aligned} |u_{\mathbf{k}}|^2 &= \frac{1}{2}\left(1 + \frac{\epsilon_{\mathbf{k}}}{E_{\mathbf{k}}}\right), \\ |v_{\mathbf{k}}|^2 &= \frac{1}{2}\left(1 - \frac{\epsilon_{\mathbf{k}}}{E_{\mathbf{k}}}\right). \end{aligned} \tag{3.63}$$

Each eigenenergy $E_{\mathbf{k}}$ is given by the two eigenvalues of the $H_{\mathbf{k}}$ matrices,

$$E_{\mathbf{k}} = \pm\sqrt{\epsilon_{\mathbf{k}}^2 + \Delta^2}. \tag{3.64}$$
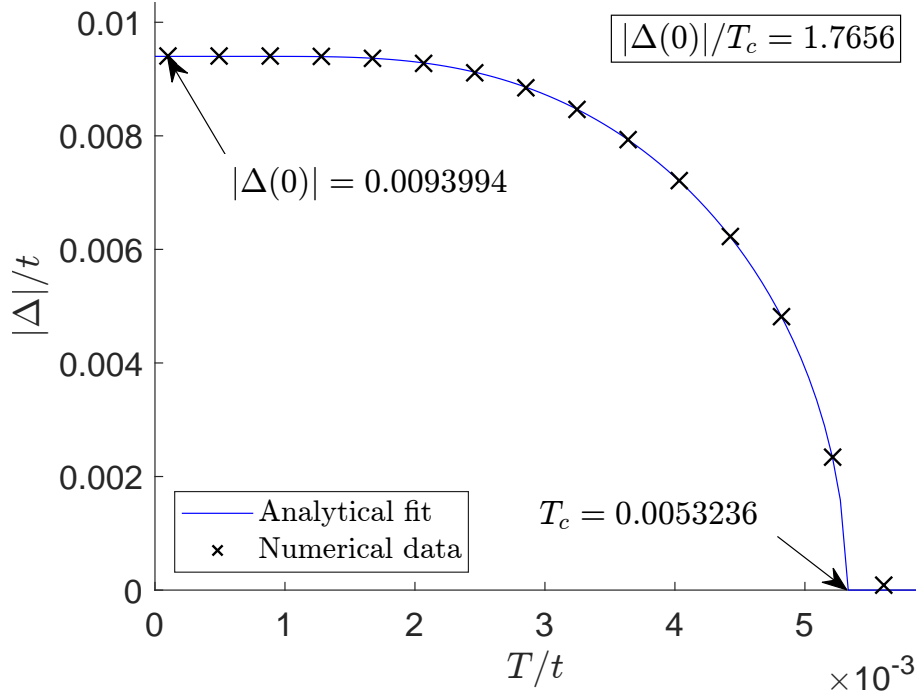
Figure 3.4: Temperature-dependence of gap parameter for a system with 50×25 lattice points. Analytical fit with fit parameter $|\Delta(0)|$ and T_c shows a very close theoretical value in Eq. (3.66). $t = 1$, $V = -0.8t$, $n = 0.35$.

Consequently, the self-consistent gap equation can be written,

$$\Delta = V \sum_{\mathbf{k}} \frac{\Delta}{2E_{\mathbf{k}}} \tanh\left(\frac{E_{\mathbf{k}}}{2k_{\mathrm{B}}T}\right). \tag{3.65}$$

By converting summation of $\mathbf{k}$ to integral of $\epsilon_{\mathbf{k}}$ and the weak-coupling limit, one will obtain the relation of the gap parameter at absolute zero $\Delta(0)$ and the critical temperature T_{c},

$$\frac{\Delta(0)}{k_{\mathrm{B}}T} = 1.765. \tag{3.66}$$

We can then use real-space BCS theory to calculate the temperature dependence of the gap parameter as shown in Fig. 3.4, one can use the relation above as a check that it holds in homogeneous gap parameters.

Chapter 4

Superconductivity subject to a magnetic field

4.1 Critical fields of superconductivity

In the superconducting state, there also exist a critical magnetic field H_c in which a phase transition to the normal state occurs. A good approximation to this is derived by Gorter and Casimir, by comparing the experimental free energy temperature dependence between a normal metal and a superconductor [27],

$$F_{\mathrm{n}} - F_{\mathrm{s}} = \Delta U - \frac{1}{2}\gamma T^2 + \frac{1}{4}\gamma T^4/T_{\mathrm{c}}^2, \tag{4.1}$$

where ΔU is the difference between the internal energy of the states, known as the condensation energy, and γ is the Sommerfeld coefficient of the electronic specific heat in a normal metal. Comparing the change in free energy with the change in free energy from Ginzburg-Landau theory in Eq. (B.5), the Gorter-Casimir formula can be derived to be,

$$H_{\mathrm{c}}(T) = H_0 \left[1 - \left(\frac{T}{T_{\mathrm{c}}} \right)^2 \right]. \tag{4.2}$$

From the equation, the critical temperature at zero magnetic field is set as $T_{\mathrm{c}} = 2(\Delta U/\gamma)^{\frac{1}{2}}$. On the other hand, the critical field at absolute zero is,

$$H_0 = (8\pi\Delta U)^{\frac{1}{2}}. \tag{4.3}$$

Furthermore, by evaluating the ground energy in the momentum-space. the condensation energy is found to be,

$$U_n - U_s = \frac{N(0)}{2}|\Delta|^2, \tag{4.4}$$

where $N(0)$ is the density of states of the normal metal around the Fermi level. The reader is referred to Tinkham, for the detailed derivation [15]. Inserting the condensation energy, one obtains

$$H_0 = \left(\frac{8\pi N(0)|\Delta|^2}{2} \right)^{\frac{1}{2}}. \tag{4.5}$$
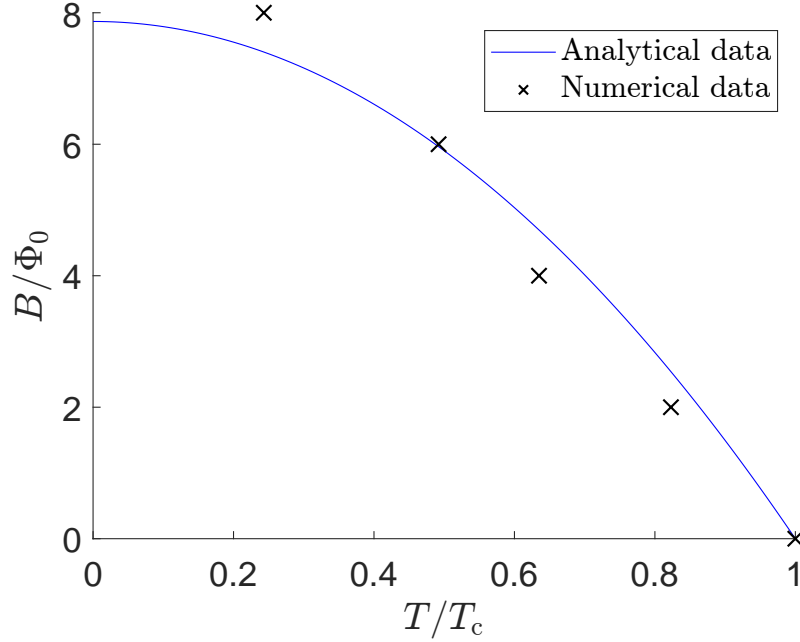
Figure 4.1: Critical magnetic field temperature-dependence, normalized by the flux quantum and the zero-field critical temperature in a system with 50×25 lattice points. The zero-field critical temperature has been fixed to the self-consistent numerical calculation, while a parameter fit is performed on H_0. The numerical data fits closely to the Gorter-Casimir formula in Eq. (4.2). $t = 1$, $V = 1.7$, $n = 0.35$.

With this equation a good estimate on the necessary magnetic field to destroy superconductivity can be obtained.

Incorporating Peierls substitution in the BCS Hamiltonian, one can self-consistently calculate the effects of magnetic fields under superconductivity and find the average superconducting order parameter across different temperatures. Evaluating the critical temperatures allows us to plot the phase diagram based on the Gorter-Casimir formula in Fig. 4.1. From the numerical fit, one obtains $\frac{H_0}{\Phi_0}{}_{\text{fit}} \approx 7.86$.

4.2 The superconducting vortex

To give rise to vortices, we shall impose the magnetic flux through the MUC to be equal to integer numbers of the flux quantum Φ_0,

$$\int_{\text{MUC}} d^2\mathbf{r}\hat{\mathbf{n}} \cdot \mathbf{B} = BL_{\text{x}}L_{\text{y}} = n\Phi_0,$$
$$\implies \frac{B}{\Phi_0} = \frac{n}{L_{\text{x}}L_{\text{y}}}, \tag{4.6}$$

where $n \in \mathbb{N}$. A Hamiltonian matrix of size $2L_{\text{x}} \times 2L_{\text{y}}$ is contructed according to Eq. (3.45). Following the algorithm in Section 3.2.5, the matrix is iteratively diagonalized numerically, and modified until a self-consistent solution of the superconducting order parameter is obtained. The attractive interaction V is set, such that $t \gg |\Delta_i|$ so that the gap bandwidth does not cover the entire of the energy band. One should
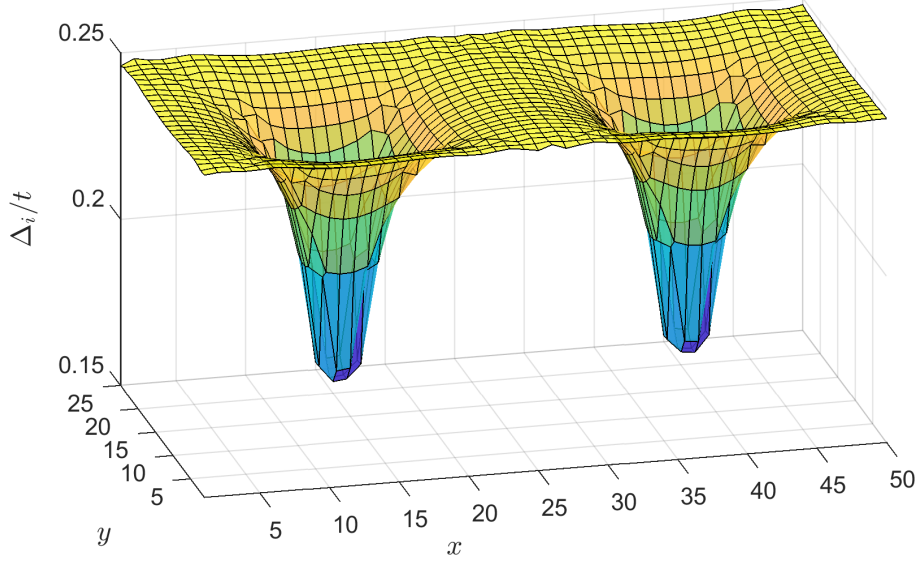
Figure 4.2: Two vortices in a MUC with 50×25 lattice points. $t = 1$, $V = 1.95t$, $k_\mathrm{B}T = 10^{-4}t$, $n = 0.35$, $B = \frac{2\Phi_0}{L_\mathrm{x}L_\mathrm{y}}$.

also take care that the free energy contribution of the applied magnetic field does not exceed the free energy change due to superconductivity, $\frac{|\Delta|^2}{V} > \frac{B^2}{8\pi}$. This relation is taken from Appendix B.

The formation of two vortices in a rectangular MUC can be observed through its superconducting order parameter in Fig. 4.2.

Throughout this chapter, the vortex state in a square lattice structure will be investigated. Its existence will be determined through the complex phase of the superconducting order parameter will be evaluated. Furthermore, several parameters analogous the phenomenological counterpart such as the coherence length and the free energy will be calculated from the BCS Hamiltonian. This will provide the basis to confirm validity of the microscopic descrition, as well as the real space numerical BCS calculations.

4.2.1 Complex phase of the order parameter

As discussed earlier, one would need to perform a gauge transformation when including the magnetic field in a tight-binding system. This corresponds to the transformation in the Wannier wavefunction. One can remedy this in the tight-binding model by transforming the hopping integral,

$$t_{ij} \to t_{ij} e^{i\frac{\pi}{\Phi_0}\theta_{ij}}. \tag{4.7}$$

It is then natural to assume, that by the definition of the interaction Hamiltonian in Eq. (3.37), one would also need a transform the attractive interaction V. However, due to the mean-field theory, this explicit treatment can be circumvented by self-consistently solving the superconducting order parameter Δ_i. Nevertheless, one can still see evidence of this transformation by observing the phase of a self-consistent superconducting order parameter.
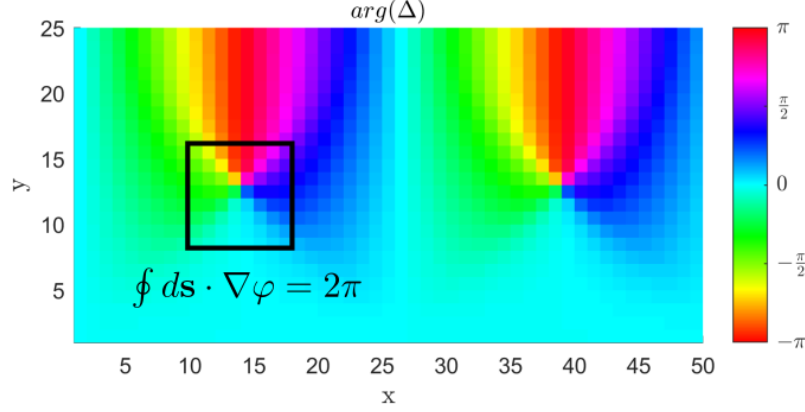
Figure 4.3: Taking a closed path integral of the gradient of the superconducting order parameter phase will lead to 2π. $t = 1$, $V = -1.7t$, $n = 0.35$, $k_{\mathrm{B}}T = 10^{-4}t$, $B = \frac{2\Phi_0}{L_{\mathrm{x}}L_{\mathrm{y}}}$.

Given a superconducting order parameter of the form $\Delta_i = |\Delta_i|e^{i\varphi(\mathbf{r}_i)}$, it is then required by Ginzburg-Landau theory and Bohr-Sommerfeld quantum condition that the complex phase $\varphi(\mathbf{r})$ follows the relation [15],

$$\oint d\mathbf{s} \cdot \nabla\varphi(\mathbf{r}) = 2\pi n, \tag{4.8}$$

where a closed integral is performed on a loop around the vortex center.

Using Lagrange interpolating polynomial as shown in Eq. (A.11), one can discretize the gradient and compute the path integral numerically,

$$\oint d\mathbf{s} \cdot \nabla\varphi(\mathbf{r}) \approx \sum_{\langle i,j\rangle \in \partial S} \Delta\varphi_{ji}, \tag{4.9}$$

where $\langle i, j\rangle \in \partial S$ is the neighboring sites along the closed path as indicated by the black lines in Fig. 4.3. The phase difference can be approximated to [28],

$$\Delta\varphi_{ji} = \frac{1}{a}\mathrm{mod}(\varphi(\mathbf{r}_j) - \varphi(\mathbf{r}_i) + \pi, 2\pi) - \pi. \tag{4.10}$$

Using this numerical approximation in Fig. (4.3), for the path integral along $(17, 17) \rightarrow (9, 17) \rightarrow (9, 9) \rightarrow (17, 9) \rightarrow (17, 17)$, one will obtain $\oint d\mathbf{s} \cdot \nabla\varphi \approx 6.2519 \approx 2\pi$.

Furthermore, one can also evaluate the phase shift between MUC boundaries. One can derive the transformation by performing a change of basis in the annihilation and creation operator,

$$c_{i\sigma} \rightarrow c_{i\sigma}e^{i\frac{\pi}{\Phi_0}\Lambda_i}, \tag{4.11}$$

Where Λ_i correspond to some gauge transformation on site i. As a consequence of the gauge transformation from Eq. (3.31), one can show a transformation in the superconducting order parameter across MUC boundaries in the y-direction to be,

$$\Delta_i = V\langle c_{i\downarrow}c_{i\uparrow}\rangle \rightarrow V\langle c_{i\downarrow}e^{i\frac{\pi}{\Phi_0}BL_{\mathrm{y}}x}c_{i\uparrow}e^{i\frac{\pi}{\Phi_0}BL_{\mathrm{y}}x}\rangle = \Delta_i e^{i\frac{2\pi}{\Phi_0}BL_{\mathrm{y}}x}. \tag{4.12}$$

Since the imposed magnetic field in Fig 4.3 corresponds to two flux quantum, this leads to the phase $4\pi\frac{x}{L_{\mathrm{x}}}$. This can be clearly observed in the phases $\varphi(x, L_{\mathrm{y}})$ for $x = 1$ and 25, where no discontinuity exists between the upper and lower boundaries of the MUC.

4.2.2 BCS coherence length

Analogous to the coherence length ξ introduced in the Ginzburg-Landau theory, the coherence length ξ_0 was also calculated by the BCS theory, and is given by [29],

$$\xi_0 = \frac{\hbar v_\mathrm{F}}{\pi \Delta(0)}, \tag{4.13}$$

where $\Delta(0)$ is the superconducting order parameter at absolute zero and v_F is the Fermi velocity obtained by the derivative of the dispersion relation at the Fermi level $v_\mathrm{F} = \frac{1}{\hbar}|\nabla_\mathbf{k}\epsilon_\mathbf{k}|_{\mathbf{k}=\mathbf{k}_\mathrm{F}}$.

As discussed in Section 2.2, such a coherence length describes the length at which the order parameter should not change appreciably. This can be interpreted as a measure of the Cooper pair size, or the vortex diameter. A detailed theoretical discussion of this can be followed in Appendix B.

Using Eq. (3.14) as the dispersion relation, the momentum derivative is obtained,

$$\nabla_\mathbf{k}\epsilon_\mathbf{k} = 2ta\left[\sin(k_\mathrm{x}a)\mathbf{e}_\mathrm{x} + \sin(k_\mathrm{y}a)\mathbf{e}_\mathrm{y}\right]. \tag{4.14}$$

In here, the the Fermi wavevector is chosen such that $\epsilon_{\mathbf{k}_\mathrm{F}} = 0$.

For a non-circular Fermi surface, one would obtain an angle-dependent coherence length $\xi_0(\theta)$. One can see the cause of this dependence in Fig. 4.4 where the magnitude of Fermi wavevectors become non-uniform along the polar angles θ of a non-circular Fermi surface.
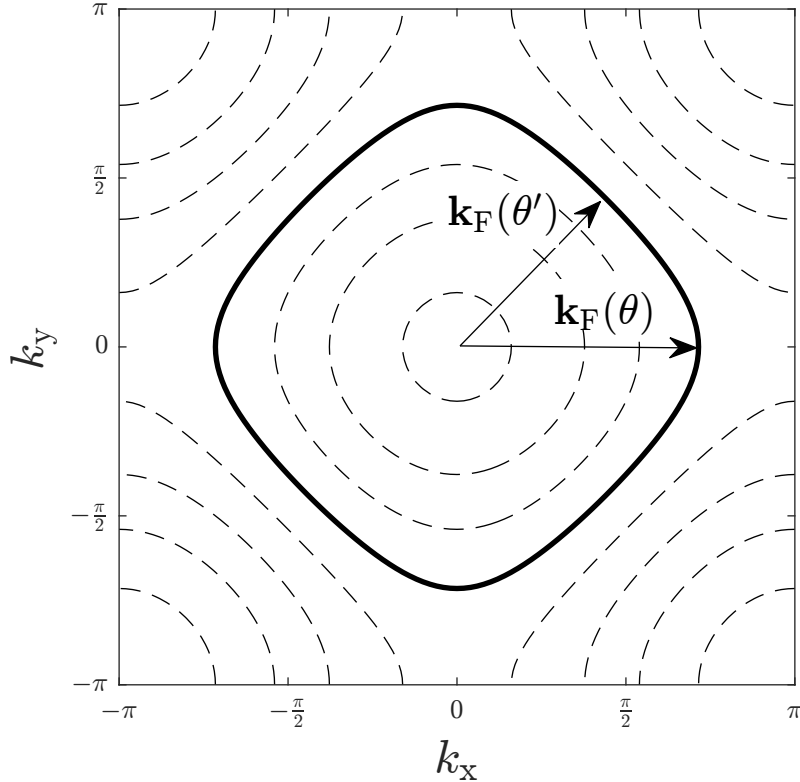

Figure 4.4: Fermi wavevector of a non-circular Fermi surface (solid line). It is shown here that generally $\mathbf{k}_\mathrm{F}(\theta) \neq \mathbf{k}_\mathrm{F}(\theta') \implies \xi_0(\theta) \neq \xi_0(\theta')$

From the above, the BCS coherence length of an atomic square lattice is,

$$\xi_0 = \frac{2ta}{\pi \Delta(0)} \sqrt{\sin^2(k_x a) + \sin^2(k_y a)}. \tag{4.15}$$

With the parameters of Fig. 4.2, at $t = 1$, $V = -1.95t$, and $\mu = -0.75t$, one obtains a superconducting order parameter of $\Delta(0) = 0.24t$. Evaluating at two angles $\theta = 0, \frac{\pi}{4}$, one obtains a value of $\xi_0(0) = 2.04$ and $\xi_0(\frac{\pi}{4}) = 3.68$. The difference in the coherence length can be explained in the square-like shape of the vortex, whereby the diameter of the vortex is longer along its diagonal rather than its sides $d_{0,\text{vortex}}(\frac{\pi}{4}) > d_{0,\text{vortex}}(0)$, where $d_{0,\text{vortex}}(\theta) = 2\xi_0(\theta)$. This is caused by the finite size effects on the vortex geometry in a square MUC. In the case of the vortex in study, the obtained coherence lengths match quite well with its respective vortex diameter, where $d_{0,\text{vortex}}(0) \approx 6$ and $d_{0,\text{vortex}}(\frac{\pi}{4}) \approx 8$.

4.2.3 Free energy and vortex lattice structure

In the beginning of the thesis, it has been mentioned that the minimization of the free energy plays a significant role in the formation of vortex lattice structures. With our BCS Hamiltonian, we can calculate the free energy F_{BCS} by taking its expectation value,

$$F_{\text{BCS}} = - \sum_{\langle i,j \rangle, \sigma}^{N} t_{ij} \langle c_{i\sigma}^\dagger c_{j\sigma} \rangle - \mu \sum_{i,\sigma}^{N} \langle c_{i\sigma}^\dagger c_{i\sigma} \rangle + V \sum_{i}^{N} \langle c_{i\uparrow}^\dagger c_{i\downarrow}^\dagger c_{i\downarrow} c_{i\uparrow} \rangle + \frac{H^2}{8\pi} - TS. \tag{4.16}$$

One can expand the interaction term using Wick's theorem, in terms of mean fields of all possible pairings [30],

$$V \sum_{i}^{N} \langle c_{i\uparrow}^\dagger c_{i\downarrow}^\dagger c_{i\downarrow} c_{i\uparrow} \rangle = V \sum_{i} \left(\langle c_{i\uparrow}^\dagger c_{i\downarrow}^\dagger \rangle \langle c_{i\downarrow} c_{i\uparrow} \rangle - \langle c_{i\uparrow}^\dagger c_{i\downarrow} \rangle \langle c_{i\downarrow}^\dagger c_{i\uparrow} \rangle \right. \tag{4.17}$$
$$\left. + \langle c_{i\uparrow}^\dagger c_{i\uparrow} \rangle \langle c_{i\downarrow}^\dagger c_{i\downarrow} \rangle \right).$$

Using Bogoliubov-de Gennes equation, one will then obtain the following free energy,

$$F_{\text{BCS}} = - \sum_{\langle i,j \rangle}^{N} t_{ij} \langle K_{ij} \rangle - \mu \langle N \rangle + \frac{1}{V} \sum_{i}^{N} |\Delta_i|^2 + V \sum_{i} \langle n_{i\uparrow} \rangle \langle n_{i\downarrow} \rangle - TS + \frac{H^2}{8\pi}$$

$$\langle K_{ij} \rangle = \sum_{k} \left[u_{ik}^* u_{jk} f(E_k) + v_{ik} v_{jk}^* f(-E_k) \right] \tag{4.18}$$

$$\langle n_{i\uparrow} \rangle \langle n_{i\downarrow} \rangle = \sum_{k,l} |u_{ik}|^2 |v_{il}|^2 f(E_k) f(-E_l),$$

where the entropy of the fermionic quasiparticles is calculated by the statistical entropy of the Fermi distributions $f(E_i)$,

$$S = -k_B \sum_{i} \left[f(E_i) \ln f(E_i) + [1 - f(E_i)] \ln (1 - f(E_i)) \right]. \tag{4.19}$$
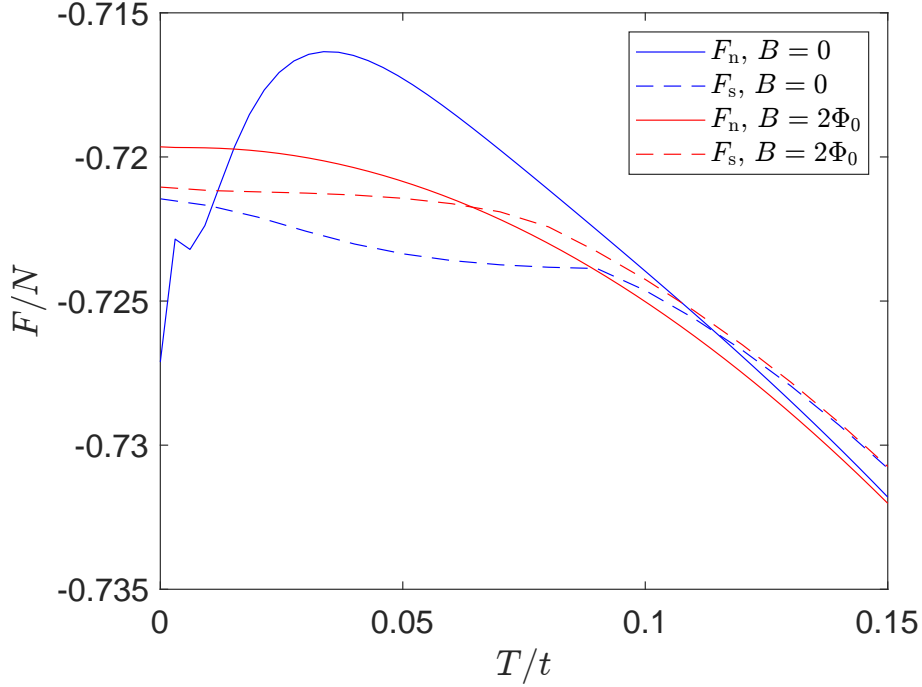
Figure 4.5: Free energy of normal and superconducting metal at various temperatures and magnetic field from the numerical calculation of BCS Theory. Initially, free energy of the superconductor is minimized, however, after surpassing a critical temperature T_c, the normal state becomes energetically preferable. $t = 1$, $V = -1.7t$, $n = 0.35$.

Calculating the free energy explicitly, one can observe that the attractive interaction term does indeed reduce the free energy. This can be seen in Fig. 4.5, where the numerical calculation of the free energy is performed for both the superconductor and the normal metal. The superconducting free energy is obtained by inserting the self-consistent superconducting order parameters and chemical potential. Diagonalization of the corresponding matrix then gives us all the required parameters to calculate the free energy. For the normal metal, one still needs to iterate a self-consistent chemical potential. However, the trivial solution $\boldsymbol{\Delta} = 0$ is introduced in the algorithm.

One can see that the numerical calculation is consistent with the free energy with the form $F \propto -T^2$ [31]. Furthermore, we can see that the superconducting free energy is indeed reduced compared to the normal metal. Above certain critical temperature T_c, the superconducting free energy overtakes the free energy of the normal metal and a phase transition occurs.

It should be acknowledged however, due to finite size effects, numerical calculation of the free energy shows a deviation in the low temperature regime $k_B T < 0.05t$. This is particularly visible in the zero-field calculations, as there are few states around the chemical potential that are accessible in low temperature. This problem could be remedied by a larger MUC size, at the cost of computation time. Therefore, exploring optimization techniques may be useful to achieve a more accurate free energy.

As an outlook, the free energy calculation can also be used to determine vortex lat-
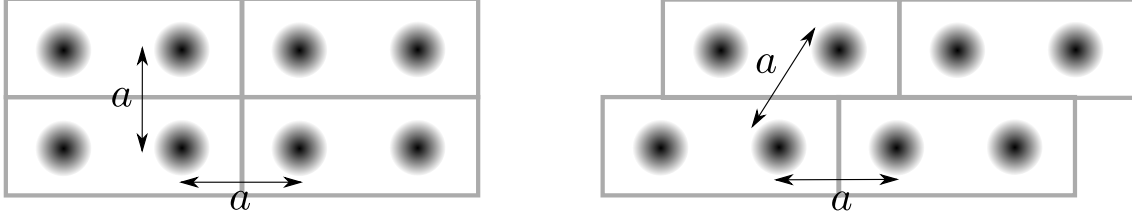
Figure 4.6: Vortex in square lattice (left) and hexagonal lattice (right). To construct a vortex lattice, one would need to connect each magnetic unit cell correctly by changing boundary hoppings such that the vortices align according to the desired structure.

tice structure that corresponds to the minimum of the energy in a similar manner to the phenomenological description. One can do this by changing the gauge transformation in the boundary hoppings as shown in Section 3.1.3, such that it correspond to the vortex lattice structure in study.

One can visualize this through the "stitching" of magnetic unit cells as shown in Fig. 4.6. For hexagonal vortex lattice, a hopping upward would correspond to hopping to a site such that a vortex will be positioned triangularly between each other.

One needs to take care that under hexagonal lattice structure, the hopping also depend on the number of flux quatum per unit cell. Furthermore, with a rectangular MUC, lattice lengths L_x and L_y have to be adjusted in such a way that the vortices form the corners of an equilateral triangle. Through simple geometry, one can deduce that in a hexagonal lattice structure for a $B = \frac{2\Phi_0}{L_x L_y} n$ with $n \in \mathbb{N}$ it is required that the approximate ratio between the lattice length is $\frac{L_y}{L_x} \approx \frac{\sqrt{3}}{4} n$. Results of preliminary calculations are displayed in Appendix C.3.

4.2.4 Convergence of the superconducting order parameter in vortex state

Obtaining a self-consistent value for the superconducting order parameter in the vortex state is generally more demanding. The complexity of the calculation is caused by the computation of the phase as well as the formation of the vortex in the superconducting order parameter. Small changes in $||\boldsymbol{\Delta} - \boldsymbol{\Delta}'||$ do not necessarily imply convergence as the superconducting order parameter is no longer uniform.

To obtain a converged value for the vortex superconducting order parameter, one would need a convergence criterion of $\epsilon_{\text{diff}} \approx 10^{-16}$. One needs to strike a balance between providing accessible states and minimizing computation time for matrix diagonalization. Alternatively, one can also set a larger attractive interaction V. However, setting a large V would not give a physically meaningful value, since interaction energy in superconductivity is at the range of $|\Delta| \ll t$. On the other hand, setting a smaller V would require a significantly higher iteration to achieve convergence.

Fig. 4.7 gives an idea of how the convergence path of the superconducting order parameter. For a MUC 50×25 lattice points, with an attractive interaction at $V = -1.95t$, one would reach several plateau in the convergence until a difference in
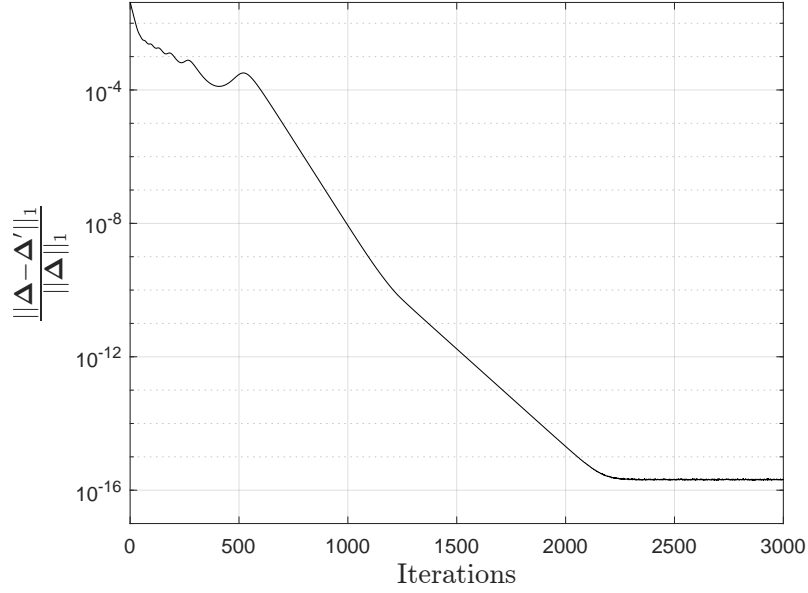
Figure 4.7: Convergence of the self-consistent superconducting order parameter. $t = 1$, $V = 1.95t$, $n = 0.35$, $B = \frac{2\Phi_0}{25 \times 50}$.

superconducting order parameter corresponding to the minimum numerical precision in the change of the superconducting order parameter is achieved. The evolution of the superconducting order parameter along the numbers of iterations can be seen in Appendix C.2.

4.3   Supercurrent

Superconductors, when subjected to magnetic fields, give rise to the supercurrent $\mathbf{J}_s$ as already discussed phenomenologically. To calculate the supercurrent, we can evaluate the current flux accross each site using the continuity equation,

$$(\boldsymbol{\nabla} \cdot \mathbf{J}_s)_i + \partial_t \hat{\rho}_i = 0, \tag{4.20}$$

whereby $\hat{\rho}_i = -e\hat{n}_i = -e \sum_\sigma c_{i\sigma}^\dagger c_{i\sigma}$. With the Heisenberg picture, one can obtain the operator time-dependent representation,

$$\partial_t \hat{n}_i = \frac{i}{\hbar} \left[\hat{H}_{\text{BCS}}, \hat{n}_i \right]. \tag{4.21}$$

Inserting the BCS Hamiltonian, one can evaluate three seperate terms,

$$
\begin{aligned}
\partial_t \hat{n}_i = -\frac{i}{\hbar} \sum_\sigma &\left(\sum_{\langle j,k \rangle, \sigma'} t_{jk} \left[c_{j\sigma'}^\dagger c_{k\sigma'}, c_{i\sigma}^\dagger c_{i\sigma} \right] + \sum_{j,\sigma'} \mu \left[c_{j\sigma'}^\dagger c_{j\sigma'}, c_{i\sigma}^\dagger c_{i\sigma} \right] \right. \\
&\left. - V \sum_j \left[c_{j\uparrow}^\dagger c_{j\downarrow}^\dagger c_{j\downarrow} c_{j\uparrow}, c_{i\sigma}^\dagger c_{i\sigma} \right] \right).
\end{aligned}
\tag{4.22}
$$

One can find that the first term is the only non-zero term, while the rest of the commutator vanishes,

$$\left[c_{j\sigma'}^\dagger c_{k\sigma'}, c_{i\sigma}^\dagger c_{i\sigma}\right] = \delta_{ki}\delta_{\sigma\sigma'}c_{j\sigma'}^\dagger c_{i\sigma} - \delta_{ji}\delta_{\sigma\sigma'}c_{i\sigma}^\dagger c_{k\sigma'}$$
$$\left[c_{j\sigma'}^\dagger c_{j\sigma'}, c_{i\sigma}^\dagger c_{i\sigma}\right] = 0 \tag{4.23}$$
$$\left[c_{j\uparrow}^\dagger c_{j\downarrow}^\dagger c_{j\downarrow} c_{j\uparrow}, c_{i\sigma}^\dagger c_{i\sigma}\right] = 0$$

giving us the time derivative of the number density operator,

$$\partial_t \hat{n}_i = -\frac{i}{\hbar} \sum_{j\in\text{nn } i,\sigma} \left(t_{ji}c_{j\sigma}^\dagger c_{i\sigma} - t_{ij}c_{i\sigma}^\dagger c_{j\sigma}\right). \tag{4.24}$$

The details of the calculation can be followed in the Appendix.

From Eq.(4.20), we get the the flux from site i,

$$(\boldsymbol{\nabla}\cdot\mathbf{J}_\text{s})_i = \frac{ie}{\hbar} \sum_{j\in\text{nn } i,\sigma} \left(t_{ji}c_{j\sigma}^\dagger c_{i\sigma} - t_{ij}c_{i\sigma}^\dagger c_{j\sigma}\right). \tag{4.25}$$

Since the current flux from site i towards a neighboring site j should be equal to the counter flux from site j to site i, we can immediately deduce from the equation above that the current flux $J_{\text{s},ji}$ to site j is,

$$J_{\text{s},ji} = \frac{ie}{\hbar} \sum_\sigma \left(t_{ji}c_{j\sigma}^\dagger c_{i\sigma} - t_{ij}c_{i\sigma}^\dagger c_{j\sigma}\right), \tag{4.26}$$

with $J_{\text{s},ji} = -J_{\text{s},ij}$.

Taking the expectation value of the current flux, one can use the Bogoliubov transformation to obtain the following,

$$\langle J_{\text{s},ji}\rangle = \frac{ie}{\hbar} \sum_{k,\sigma} \left[t_{ji}\left\{ u_{jk\sigma}^* u_{ik\sigma} f(E_{k\sigma}) + v_{jk\sigma} v_{ik\sigma}^* \left[1 - f(E_{k\bar\sigma})\right] \right\} \right.$$
$$\left. - t_{ij}\left\{ u_{ik\sigma}^* u_{jk\sigma} f(E_{k\sigma}) + v_{ik\sigma} v_{jk\sigma}^* \left[1 - f(E_{k\bar\sigma})\right] \right\} \right]. \tag{4.27}$$

In similar manner to the way one obtains the gap equation in Section 3.2.4, one can use the Bogoliubov-de Gennes equation to suppress the spin index in the eigenenergy,

$$\langle J_{\text{s},ji}\rangle = \frac{ie}{\hbar} \sum_k \left\{ \left[t_{ji}u_{jk\uparrow}^* u_{ik\uparrow} - t_{ij}u_{ik\uparrow}^* u_{jk\uparrow} \right] f(E_{k\uparrow}) \right.$$
$$\left. + \left[t_{ji}v_{jk\downarrow}v_{ik\downarrow}^* - t_{ij}v_{ik\downarrow}v_{jk\downarrow}^* \right] f(-E_{k\uparrow}) \right\}. \tag{4.28}$$

By summing all the direction of the current flux we get the supercurrent vector $\mathbf{J}_{\text{s},i}$,

$$\mathbf{J}_{\text{s},i} = \sum_{k=\text{x,y}} \left(\langle J_{\text{s},ik+}\rangle - \langle J_{\text{s},ik-}\rangle\right)\mathbf{e}_k \tag{4.29}$$

one obtain the supercurrent as shown in Fig. 4.8.

As a comparison, one can also use Maxwell's equation, $\mathbf{J} = \frac{c}{4\pi}\boldsymbol{\nabla} \times \mathbf{B}$ to generate supercurrent $\mathbf{J}_{\text{s,phenom}}$ formed by the vortex field distribution from the phenomenological description in Eq. (2.19),

$$\mathbf{J}_{\text{s,phenom}}(\mathbf{r}) = \frac{B_{\text{a}}c}{4\pi}\sum_{j}\frac{e^{i\mathbf{Q}_j\cdot\mathbf{r}}}{1 + \lambda^2\mathbf{Q}_j^2}i(\mathbf{Q}_j \times \mathbf{e}_{\text{z}}). \tag{4.30}$$

By taking a large $\lambda \gg 1$, one can generate the phenomenological supercurrent. With this one can see that the numerical calculation of the supercurrent from the BCS theory indeed takes a similar form to the supercurrent derived from the phenomenological description shown in Fig. 4.9. However, it is clear that as one leaves the vortex center in the phenomenological description, the current vanishes rapidly. This is caused by the high-κ approximation that have been taken earlier, which allows us to write vortices as a Dirac delta functions. In this regard, we have also shown the clear advantage of the BCS theory to provide a more physically meaningful result of the supercurrent.

4.3.1 Self-consistent vector potential

The supercurrent as shown in Fig. 4.8 will induce a vector potential in the system. Through Maxwell's equation, one can calculate the vector potential of the supercurrent $\mathbf{A}_{\text{s}}$ [32],

$$\mathbf{A}_{\text{s}}(\mathbf{r}) = \frac{1}{c}\int d^2\mathbf{r}'\frac{\mathbf{J}_{\text{s}}(\mathbf{r}')}{|\mathbf{r} - \mathbf{r}'|}. \tag{4.31}$$

Calculating the magnetic vector potential from the supercurrent is generally not trivial, as one would need to solve a 2D Poisson equation. Nevertheless, a vector potential can be obtained from finite element analysis with the use of triangular nodes [33]. Given the vector potential, one can obtain a more physically meaningful approximation by including the supercurrent in the self-consistent calculation of the superconducting order parameter, where the total vector potential $\mathbf{A}$ is,

$$\mathbf{A} = \underbrace{\mathbf{A}_{\text{a}}}_{\boldsymbol{\nabla}\times\mathbf{A}_{\text{a}}=B\mathbf{e}_{\text{z}}} + \mathbf{A}_{\text{s}}. \tag{4.32}$$
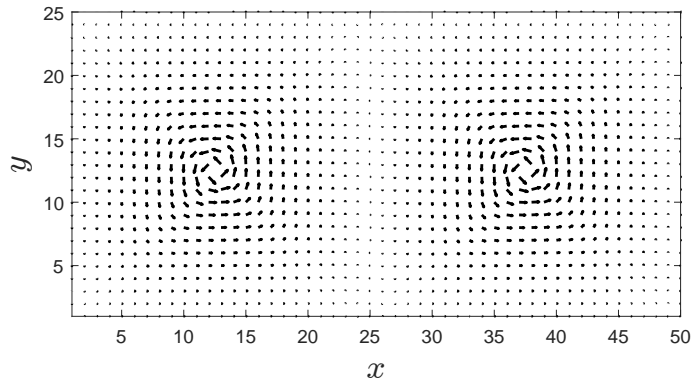

Figure 4.8: Supercurrent of a vortex state. $t = 1$, $V = -1.95t$, $n = 0.35$, $B = \frac{2\Phi_0}{25\times50}$.
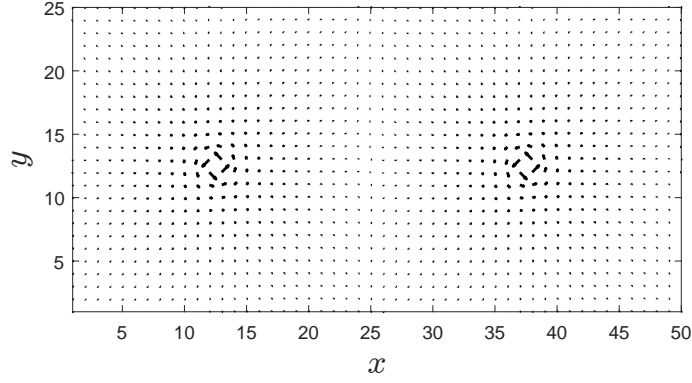
Figure 4.9: Phenomenological supercurrent of a vortex state. $\lambda = 5$, $B_{\mathrm{a}} = 1$.

From this it follows that the assumption on the homogeneity of the magnetic field breaks down. This leads to a non-trivial gauge function of the Peierls substitution, since the fields vary significantly near vortex centers.

With this, one can include the update of the vector potential in our iterative method in Section 3.2.5 along with the Bogoliubov-de Gennes equations to get a self-consistent vector potential along with its superconducting order parameter. One should be wary that this may lead in an increase to the complexity of the self-consistent algorithm, which requires further studies.

4.4   Impurities

Impurities can be introduced to represent inhomogeneity in the material. This corresponds to adding an impurity term to the Hamiltonian which essentially describes an on-site chemical potential,

$$\hat{V}_{\mathrm{imp}} = \sum_{i,\sigma} V_{\mathrm{imp},i} c_{i\sigma}^{\dagger} c_{i\sigma}, \tag{4.33}$$

where $V_{\mathrm{imp},i} > 0$ represents an on-site repulsive potential, while $V_{\mathrm{imp},i} < 0$ is an attractive potential. There is also the so-called magnetic impurity, where one introduce a potential that depends on the spin quantum number.

When introducing impurities in our s-wave superconductor, a local deformation in the superconducting order parameter may arise, in which superconductivity is suppressed on the site of the impurity. On the other hand, superconducting order parameters will increase in neighboring sites. This characteristic of the impurity can be seen in Fig. 4.10, where a single impurity potential is introduced in a superconductor.

Physically, this can occur due to the congestion of electrons generated along the neighboring site as particles are prevented from entering through the potential barrier generated by the impurity.
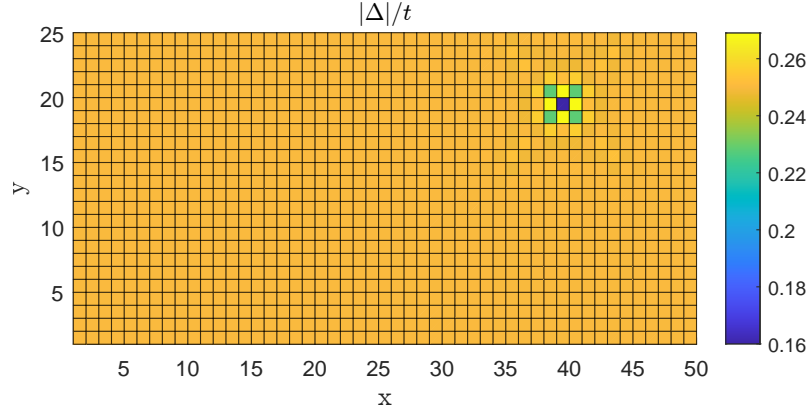
Figure 4.10: Superconducting order parameter deformation due to impurity at position $\mathbf{r} = (38, 19)$. $t = 1$, $V = -1.95t$, $B = 0$.

4.4.1 Flux pinning

Superconducting vortices are also influenced when an impurity is introduced in a system. Since an impurity may locally suppress superconductivity, to minimize the free energy, a vortex will position itself in such a way the the energetic contribution of the superconducting order parameter $\sum_i |\Delta_i|^2 / V$ is minimized. As a result, a vortex will position itself at the local suppression caused by impurity.

Flux pinning plays a crucial role in maintaining a large critical current to prevent energy dissipation caused by the Lorentz force subjected to the vortices.

This can be observed in Fig. 4.11, where the vortex center is positioned at the location of the impurity. Consequently, due to interactions between vortices, which can also be seen as other vortex readjust its position accordingly to the position of the flux pinned vortex.
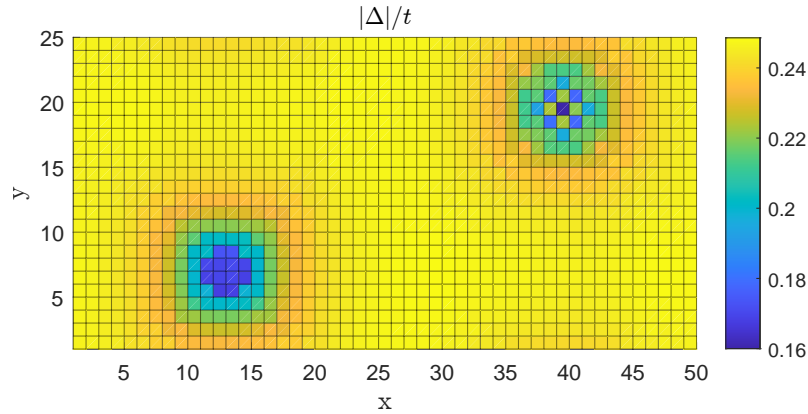

Figure 4.11: Flux pinning of a vortex at position of impurity $\mathbf{r} = (38, 19)$. $t = 1$, $V = -1.95t$, $B = \frac{2\Phi_0}{L_x L_y}$.

Chapter 5

Conclusion and Outlook

Throughout this thesis, the behaviour of conventional superconductors when subjected to a magnetic field has been investigated. Analogies from the phenomenological description and an extensive investigation of the real-space microscopic model of conventional superconductors were explored with the intention of obtaining a theoretical description that may be suited for practical applications.

Initially, the phenomenological description of superconductivity is presented in Chapter 2 to obtain some fundamental properties of the superconductors in magnetic field. Through the London equations, one can observe the attenuation of a magnetic field, vortex lattice structures and the free energy behaviour of vortices in a system.

At the start of Chapter 3, we develop a description of the tight-binding model in magnetic fields. This is done by introducing Peierls' substitution and periodic boundary conditions in the hopping integral of a tight binding model. A numerical calculation of the eigenenergies gives rise to sub-bands in the energy spectrum as shown in the Hofstatder's butterfly (see Fig. 3.2).

The real-space BCS Hamiltonian with s-wave superconductivity is constructed in the latter sections of Chapter 3. Through the use of the real-space Bogoliubov-de Gennes equations and a gap self-consistency iterative method, it is shown that one is able to obtain a real-space picture of superconductivity. Through the temperature dependence of the gap parameter Δ, one can then observe that it is indeed consistent with its momentum-space counterpart.

Finally, Chapter 4 explores different behaviours of superconductor in a magnetic field. As one would expect, the superconducting vortex would arise when a field corresponding the integer numbers of the flux quantum $n\Phi_0$ is introduced. The existence of these vortices can be confirmed by the change in the magnitude of the gap parameter and a total phase difference of $\oint \nabla \varphi = 2\pi$ around the vortex center.

From this, the minimum free energy, supercurrent and impurity effects on the vortex state is studied. Indeed, one may find that the superconducting state in fact, reduces the free energy of an interacting electronic system, at which it becomes smaller than the normal state free energy below a certain critical temperature T_c. The supercurrent generating the vortex can also be found using the continuity equation and the Bogoliubov-de Gennes equation. It is also that the supercurrent formed, resembles that of the rough high-κ approximation from the phenomenological model.

Furthermore, one also finds that the introduction of an impurity may result in the rise of flux pinning, which is desirable for many practical applications in type-II superconductors.

Through this thesis, a deeper understanding of the vortex state along with the nuances of its implementation have been obtained. It is quite clear that the real-space BCS calculations of conventional superconductors in magnetic fields is entirely consistent with its phenomenological counterparts such as the London equations and GL theory.

There are several propositions to extend the numerical calculations of the vortex state. One of this may be to incorporate the hexagonal vortex structure in the MUC as including the induced field from vortex supercurrent in the self-consistent iterative method. Furthermore, it is also of interest to study in more detail the vortex lattice structure through the "supercell method" [24].

As an outlook of this thesis, several avenues of research may be explored. One can further extend the study of the effect of magnetic field for p-wave superconductors. This may help discover the mechanisms behind novel superconductors such as the so-called "Lazarus superconductivity", where magnetic field-boosted superconductivity has been found to be associated with spin-triplet pairings [34]. Furthermore, an efficient self-consistent iterative method may be needed to accelerate convergence of the vortex state. Investigating the effect of Nagai's polynomial expansion method and Sakurai's contour integral method in solving the Bogoliubov-de Gennes equation for the convergence of the vortex may prove useful [35].

Appendix A

Derivations and Proofs

A.1   Ohm's law in a steady supercurrent

Under Ohm's law, we know that a current relates to an electric field with a conductivity tensor,

$$\mathbf{J} = \hat{\sigma}\mathbf{E}. \tag{A.1}$$

Now assuming we have a finite steady supercurrent $\mathbf{J_s} = const.$, the above should hold if Ohm's law is valid in a superconducting state. This can be done by evaluating the electric field using Helmholtz theorem, which states that one can write a vector field that vanishes at infinity as a sum of two parts, the irrotational and the transverse part [36],

$$\mathbf{E} = -\nabla\Phi + \nabla \times \mathbf{A}. \tag{A.2}$$

From the above, the scalar and vector field can be isolated,

$$\Phi = \frac{1}{4\pi} \int \frac{\nabla \cdot \mathbf{E}}{|\mathbf{r} - \mathbf{r}'|} d^3\mathbf{r}' \quad \mathbf{A} = \frac{1}{4\pi} \int \frac{\nabla \times \mathbf{E}}{|\mathbf{r} - \mathbf{r}'|} d^3\mathbf{r}'. \tag{A.3}$$

By inserting Maxwell and London equation, to the above, we get

$$\Phi = \int \frac{\rho}{|\mathbf{r} - \mathbf{r}'|} d^3\mathbf{r}' \quad \mathbf{A} = \frac{\lambda^2}{4\pi} \int \frac{\nabla \times \partial_t(\Lambda\mathbf{J_s})}{|\mathbf{r} - \mathbf{r}'|} d^3\mathbf{r}'. \tag{A.4}$$

From our assumption of a steady supercurrent, we then have $\partial_t(\mathbf{J}_s) = 0$ and $\rho = 0$. This implies, that both irrotational and transverse part vanishes, which also means $\mathbf{E} = 0$.

Following Ohm's law, we then get $\mathbf{J_s} = 0$. However, this contradicts our initial assumption that the supercurrent is constant. Therefore, Ohm's law, does not hold in a superconductor.

A.2   Change of the free energy in a vortex

As introduced in Section 2.2.3, we have the integral,

$$\frac{F - F_{\text{s0}}}{L}\bigg|_{\text{s. v.}} = \frac{1}{8\pi} \int_{0 < |\mathbf{r}| \leq r'} d^2\mathbf{r}[\mathbf{B}^2 + \lambda^2(\nabla \times \mathbf{B})^2]. \tag{A.5}$$

We shall now evaluate the second term of the integral using Einstein notation, where we use Levi-Civita symbol $\epsilon_{ijk} = \mathbf{e}_i \cdot (\mathbf{e}_j \times \mathbf{e}_k)$, Kronecker delta $\delta_{ij} = \mathbf{e}_i \cdot \mathbf{e}_j$, and summing over dummy indices,

$$(\boldsymbol{\nabla} \times \mathbf{B})^2 = \epsilon_{ijk}\epsilon_{ilm}\partial_j(B_k)\partial_l(B_m). \tag{A.6}$$

With the product rule for partial differentiation we can seperate the products to two sums. Additionally, using the properties of the Levi-Civita symbol, we can flip indices under even permutation $\epsilon_{ijk} \to \epsilon_{jki}$ for the first term and under odd permutation $\epsilon_{ijk} \to -\epsilon_{kji}$ for the second term. With these indices, one can transform it back to the vector notation,

$$\begin{aligned}
(\boldsymbol{\nabla} \times \mathbf{B})^2 &= \epsilon_{ijk}\epsilon_{ilm}[\partial_j(B_k\partial_l(B_m)) - B_k\partial_j(\partial_l(B_m))] \\
&= \epsilon_{jki}\epsilon_{ilm}\partial_j(B_k\partial_l(B_m)) + \epsilon_{kji}\epsilon_{ilm}B_k\partial_j(\partial_l(B_m)) \\
&= \nabla \cdot [\mathbf{B} \times (\boldsymbol{\nabla} \times \mathbf{B})] + \mathbf{B} \cdot [\boldsymbol{\nabla} \times \boldsymbol{\nabla} \times \mathbf{B}].
\end{aligned} \tag{A.7}$$

Inserting the above to Eq. (A.5), we get

$$\begin{aligned}
\frac{F - F_{s0}}{L}\bigg|_{\text{s. v.}} = &\frac{1}{8\pi} \int_{0 < |\mathbf{r}| \leq r'} d^2\mathbf{r}[\mathbf{B}^2 + \lambda^2(\mathbf{B} \cdot \boldsymbol{\nabla} \times \boldsymbol{\nabla} \times \mathbf{B})] \\
&+ \frac{1}{8\pi} \int_{0 < |\mathbf{r}| \leq r'} d^2\mathbf{r}\nabla \cdot [\mathbf{B} \times (\boldsymbol{\nabla} \times \mathbf{B})].
\end{aligned} \tag{A.8}$$

In the second term, we use the divergence theorem for the special case of a plane, where for some vector field $\mathbf{F}$, one can transform a surface integral along a surface into a closed line integral along the normal of the surface [36],

$$\int_S d^2\mathbf{r}\nabla \cdot \mathbf{F} = \oint_{\partial S} ds\mathbf{F} \cdot \hat{\mathbf{n}}. \tag{A.9}$$

Due to the vortex's tube-like structure, it is convenient to use a cylindrical coordinate system, in which we take the normal to be the radial unit vector $\hat{\mathbf{n}} = \mathbf{e}_r$. This in return, gives us the integral shown in Eq. (2.25),

$$\frac{F - F_{s0}}{L}\bigg|_{\text{s.v.}} = \frac{1}{8\pi} \int_{0 < |\mathbf{r}| \leq r'} d^2\mathbf{r}|\mathbf{B}|\Phi_0\delta^2(\mathbf{r}) + \frac{\lambda^2}{8\pi} \oint_{|\mathbf{r}|=r'} ds(\mathbf{B} \times \boldsymbol{\nabla} \times \mathbf{B}) \cdot \mathbf{e}_r. \tag{A.10}$$

A.3 Finite-difference approximation of the Laplacian

For the specific case of nearest neighbor interactions, the Laplacian on the wavefunction $\nabla^2\phi(r)$ can be solved quite explicitly with numerical differentiation and finite-difference approximation. This involves the usage of Lagrange interpolating polynomials $P_n(x)$ to approximate some function $f(x)$ along known points x_i,

$$f(x) = P_n(x) + \frac{f^{(n+1)}(\xi(x))}{(n+1)!} \prod_{i=0}^{N}(x - x_i). \tag{A.11}$$

The second term of the approximation is the error function, where $\xi(x)$ is some number that lies between the smallest interval that contains points x_i and x. The interpolating polynomial has the form,

$$P_n(x) = \sum_{i=0}^{n} f(x_i) L_i(x)$$
$$L_i(x) = \prod_{j=0, j \neq i}^{n} \frac{x - x_j}{x_i - x_j},$$

(A.12)

whereby setting x to some point x_i will lead to $P_n(x_i) = f(x_i)$, since $L_i(x_j) = \delta_{ij}$. A function, and consequently its derivatives, can then be approximated to a close degree through the Lagrange polynomial, $f(x) \approx P_n(x) \Rightarrow \partial_x^2 f(x) \approx \partial_x^2 P_n(x)$. This is in particular true for the derivatives if we set the interpolating points to be some close distance h around x_0 (i.e. $x_0 - 2h, x_0 - h, x_0, x_0 + h...$) [37].

From a 3-point approximation of a double derivative one gets,

$$\partial_x^2 f(x_0) \approx \frac{f(x_0 - h) - 2f(x_0) + f(x_0 + h)}{h^2}.$$

(A.13)

Applying this to the wave function and extending to multiple dimensions, we choose h to be on the direction of the primitive unit vectors $\mathbf{a}_i$,

$$\nabla^2 \phi(\mathbf{r}) = \frac{1}{a^2}[\phi(\mathbf{r} - \mathbf{a}_1) + \phi_\sigma(\mathbf{r} - \mathbf{a}_2) - 4\phi(\mathbf{r})$$
$$+ \phi(\mathbf{r} + \mathbf{a}_1) + \phi(\mathbf{r} + \mathbf{a}_2)].$$

(A.14)

A.4 Fourier transform and anti-commutation relations

From Eq. (3.4),

$$c_{i\sigma} = \frac{1}{\sqrt{N}} \sum_{\mathbf{k} \in \text{B.Z.}} e^{-i\mathbf{k} \cdot \mathbf{r_i}} c_{\mathbf{k}\sigma}.$$

(A.15)

With the help of the fermionic anti-commutation relation in Eq. (1.10) we can evaluate each anticommutation rules in Eq. (3.5) we have,

$$
\begin{aligned}
\{c_{\mathbf{i}\sigma}^\dagger, c_{\mathbf{j}\sigma'}\} &= \frac{1}{N} \sum_{\mathbf{k},\mathbf{k}'\in\text{B.Z.}} e^{i(\mathbf{k}\cdot\mathbf{r_i}-\mathbf{k}'\cdot\mathbf{r_j})} \{c_{\mathbf{k}\sigma}^\dagger, c_{\mathbf{k}'\sigma'}\} \\
&= \frac{1}{N} \sum_{\mathbf{k},\mathbf{k}'\in\text{B.Z.}} e^{i(\mathbf{k}\cdot\mathbf{r_i}-\mathbf{k}'\cdot\mathbf{r_j})} \delta_{\mathbf{kk}'}\delta_{\sigma\sigma'} \\
&= \frac{1}{N} \sum_{\mathbf{k}\in\text{B.Z.}} e^{i(\mathbf{k}\cdot(\mathbf{r_i}-\mathbf{r_j})} \delta_{\sigma\sigma'} \\
&= \delta_{\mathbf{ij}}\delta_{\sigma\sigma'}, \\
\{c_{\mathbf{i}\sigma}^\dagger, c_{\mathbf{j}\sigma'}^\dagger\} &= \frac{1}{N} \sum_{\mathbf{k},\mathbf{k}'\in\text{B.Z.}} e^{i(\mathbf{k}\cdot\mathbf{r_i}-\mathbf{k}'\cdot\mathbf{r_j})} \{c_{\mathbf{k}\sigma}^\dagger, c_{\mathbf{k}'\sigma'}^\dagger\} \\
&= 0, \\
\{c_{\mathbf{i}\sigma}, c_{\mathbf{j}\sigma'}\} &= \frac{1}{N} \sum_{\mathbf{k},\mathbf{k}'\in\text{B.Z.}} e^{i(\mathbf{k}\cdot\mathbf{r_i}-\mathbf{k}'\cdot\mathbf{r_j})} \{c_{\mathbf{k}\sigma}, c_{\mathbf{k}'\sigma'}\} \\
&= 0.
\end{aligned}
\tag{A.16}
$$

In the first anti-commutation relation, the Kronecker delta is obtained through a geometric sum analogous to Section A.5.

A.5 Kronecker delta from exponential sum

Without loss of generality, we assume a discretized real-space with integer coordinate $(x,y) \in [1,L_x] \times [1,L_y]$, wher $N = L_x L_y$ is the system size. With the Born-von Karman boundary condition, we impose a discretized reciprocal coordinate $(k_x, k_y) = (\frac{2\pi n}{L_x}, \frac{2\pi m}{L_y})$, with $n, m \in \mathbb{Z}$. Beginning with the summation of exponentials, we can write it as a product for the x- and y-dependencies which factorize as follows,

$$
\begin{aligned}
\sum_i e^{i(\mathbf{k}-\mathbf{k}')\cdot\mathbf{r_i}} &= \sum_{x=1}^{L_x}\sum_{y=1}^{L_y} e^{i(k_x-k_x')x} e^{i(k_y-k_y')y} \\
&= \left(\sum_{x=1}^{L_x} e^{i(k_x-k_x')x}\right)\left(\sum_{y=1}^{L_y} e^{i(k_y-k_y')y}\right).
\end{aligned}
\tag{A.17}
$$

Evaluating the sum across x, we have two cases. For $k_x = k_x'$, this trivially lead to $\sum_x^{L_x} = L_x$. As for the case $k_x \neq k_x'$, one can compute this as a geometric series,

$$
\begin{aligned}
\sum_{x=1}^{L_x} e^{i(k_x-k_x')x} &= \frac{e^{i(k_x-k_x')(L_x+1)} - e^{i(k_x-k_x')}}{e^{i(k_x-k_x')} - 1} \\
&= e^{i(k_x-k_x')} \frac{e^{i(k_x-k_x')L_x} - 1}{e^{i(k_x-k_x')} - 1}
\end{aligned}
\tag{A.18}
$$

Note that $k_x - k_x' = \frac{2\pi(n-m)}{L_x} = \frac{2\pi l}{L_x}$, where $l \in \mathbb{Z}/\{0\}$. By inserting k_x explicitly, one can see that the one will obtain $e^{i2\pi l} = 1$ for exponential term in the numerator

regardless of k_x and k'_x. This meant that for the case $k_x \neq k'_x$, the summation vanishes. Therefore, the sum across x becomes,

$$\sum_{x=1}^{L_x} e^{i(k_x - k'_x)x} = \delta_{k_x k'_x} L_x \tag{A.19}$$

Repeating the sum for the y-component in the initial sum will lead to,

$$\sum_i e^{i(\mathbf{k} - \mathbf{k}') \cdot \mathbf{r}_i} = \delta_{k_x k'_x} \delta_{k_y k'_y} L_y L_x = \delta_{\mathbf{kk}'} N \tag{A.20}$$

A.6 Peierls substitution: Gradient of the gauge function

We take the gradient of the gauge function Λ_i in Eq. (3.18),

$$\nabla \Lambda_i(\mathbf{r}) = \int_0^1 d\lambda \nabla \left[(\mathbf{r} - \mathbf{r}_i) \cdot \mathbf{A}(\mathbf{r}_i + \lambda(\mathbf{r} - \mathbf{r}_i)) \right]. \tag{A.21}$$

We shall now derive the vector calculus identity of $\nabla(\mathbf{A} \cdot \mathbf{B})$. We can show that,

$$\begin{aligned}
\mathbf{A} \times \boldsymbol{\nabla} \times \mathbf{B} &= \mathbf{e}_i \epsilon_{ijk} \epsilon_{klm} A_j \partial_l(B_m) \\
&= \mathbf{e}_i (\delta_{il}\delta_{jm} - \delta_{im}\delta_{jl}) A_j \partial_l(B_m) \\
&= \mathbf{e}_i [A_j \partial_i(B_j) - A_j \partial_j(B_i)].
\end{aligned} \tag{A.22}$$

Using the product rule we get,

$$\begin{aligned}
\mathbf{A} \times \boldsymbol{\nabla} \times \mathbf{B} &= \mathbf{e}_i [\partial_i(A_j B_j) - B_j \partial_i(A_j) - A_j \partial_j(B_i)] \\
&= \nabla(\mathbf{A} \cdot \mathbf{B}) - \nabla_{\mathbf{A}}(\mathbf{B} \cdot \mathbf{A}) - (\mathbf{A} \cdot \nabla)\mathbf{B}.
\end{aligned} \tag{A.23}$$

The gradient on the second term is acting purely on $\mathbf{A}$. Switching the vector around one will then get,

$$\mathbf{B} \times \boldsymbol{\nabla} \times \mathbf{A} = \nabla(\mathbf{A} \cdot \mathbf{B}) - \nabla_{\mathbf{B}}(\mathbf{A} \cdot \mathbf{B}) - (\mathbf{B} \cdot \nabla)\mathbf{A}. \tag{A.24}$$

Summing both cases together and noting that $\nabla(\mathbf{A} \cdot \mathbf{B}) = \nabla_{\mathbf{A}}(\mathbf{A} \cdot \mathbf{B}) + \nabla_{\mathbf{B}}(\mathbf{A} \cdot \mathbf{B})$ leads to,

$$\nabla(\mathbf{A} \cdot \mathbf{B}) = (\mathbf{B} \cdot \nabla)\mathbf{A} + (\mathbf{A} \cdot \nabla)\mathbf{B} + \mathbf{A} \times \boldsymbol{\nabla} \times \mathbf{B} + \mathbf{B} \times \boldsymbol{\nabla} \times \mathbf{A}. \tag{A.25}$$

Applying the identity above to Eq. (A.21), we have,

$$\begin{aligned}
\nabla \Lambda_i(\mathbf{r}) = \int_0^1 d\lambda [&((\mathbf{r} - \mathbf{r}_i) \cdot \nabla)\mathbf{A} + (\mathbf{A} \cdot \nabla)(\mathbf{r} - \mathbf{r}_i) \\
&+ \mathbf{A} \times \boldsymbol{\nabla} \times (\mathbf{r} - \mathbf{r}_i) + (\mathbf{r} - \mathbf{r}_i) \times \boldsymbol{\nabla} \times \mathbf{A}].
\end{aligned} \tag{A.26}$$

The first term can be rewritten by using integration by part and parametrization of $\mathbf{r}' = \mathbf{r}_i + \lambda(\mathbf{r} - \mathbf{r}_i)$ we will obtain,

$$\begin{aligned}
\int_0^1 d\lambda \mathbf{A}(\mathbf{r}_i + \lambda(\mathbf{r} - \mathbf{r}_i)) &= \left[\lambda \mathbf{A}(\mathbf{r}_i + \lambda(\mathbf{r} - \mathbf{r}_i)) \right]_0^1 - \int_0^1 d\lambda \lambda \frac{d(\mathbf{A}(\mathbf{r}_i + \lambda(\mathbf{r} - \mathbf{r}_i)))}{d\lambda} \\
&= \mathbf{A}(\mathbf{r}) - \int_0^1 d\lambda \lambda \frac{d\mathbf{r}'}{d\lambda} \cdot \nabla_{\mathbf{r}'} \mathbf{A}(\mathbf{r}').
\end{aligned} \tag{A.27}$$

Using $\nabla_{\mathbf{r}'}\mathbf{A}(\mathbf{r}') = \frac{1}{\lambda}\nabla_{\mathbf{r}}\mathbf{A}(\mathbf{r}')$, we end up with,

$$\int_0^1 d\lambda((\mathbf{r} - \mathbf{r}_i) \cdot \nabla)\mathbf{A} = \mathbf{A}(\mathbf{r}) - \int_0^1 d\lambda\mathbf{A}(\mathbf{r}_i + \lambda(\mathbf{r} - \mathbf{r}_i)). \tag{A.28}$$

For the rest of the term, we know that $(\mathbf{A} \cdot \nabla)\mathbf{r} = \mathbf{A}$, $\nabla \times \mathbf{r} = 0$, and $\nabla \times \mathbf{A} = \mathbf{B}$, we have,

$$\nabla\Lambda_i(\mathbf{r}) = \mathbf{A}(\mathbf{r}) + \int_0^1 d\lambda\lambda[\cancel{-\mathbf{A} + \mathbf{A}} + (\mathbf{r} - \mathbf{r}_i) \times \mathbf{B}]$$
$$= \mathbf{A}(\mathbf{r}) + \int_0^1 d\lambda\lambda(\mathbf{r} - \mathbf{r}_i) \times \mathbf{B}. \tag{A.29}$$

Since we have assumed a homogenous external field $\mathbf{B} = \mathbf{B}_a$, the magnetic field can be taken outside the integral. Furthermore, by using the Wannier basis, we also assumed a high localized atomic orbital which means $\mathbf{r} \approx \mathbf{r}_i$. Therefore the second term in Eq. (A.29) can be neglected.

Hence this gives us,

$$\nabla\Lambda_i(\mathbf{r}) \approx \mathbf{A}(\mathbf{r}). \tag{A.30}$$

A.7 Commutation relation in supercurrent

As we have seen in Eq. (4.23), to get the form of the supercurrent under Bogoliubov transformation, one needs to evaluate the commutation relations, $\left[c_{j\sigma'}^\dagger c_{k\sigma'}, c_{i\sigma}^\dagger c_{i\sigma}\right]$, $\left[c_{j\sigma'}^\dagger c_{j\sigma'}, c_{i\sigma}^\dagger c_{i\sigma}\right]$, and $\left[c_{j\uparrow}^\dagger c_{j\downarrow}^\dagger c_{j\downarrow} c_{j\uparrow}, c_{i\sigma}^\dagger c_{i\sigma}\right]$.

For the first term, we will use the following commutator identity,

$$[AB, CD] = A\{B, CD\} - \{A, CD\}B$$
$$= A\{B, C\}D - \{A, C\}BD + CA\{B, D\} - C\{A, D\}B. \tag{A.31}$$

Inserting the annihlation and creation operators we have,

$$\left[c_{j\sigma'}^\dagger c_{k\sigma'}, c_{i\sigma}^\dagger c_{i\sigma}\right] = c_{j\sigma'}^\dagger \underbrace{\{c_{k\sigma'}, c_{i\sigma}^\dagger\}}_{\delta_{ki}\delta_{\sigma\sigma'}} c_{i\sigma} - \underbrace{\{c_{j\sigma'}^\dagger, c_{i\sigma}^\dagger\}}_{0} c_{k\sigma'} c_{i\sigma}$$
$$+ c_{i\sigma}^\dagger c_{j\sigma'}^\dagger \underbrace{\{c_{k\sigma'}, c_{i\sigma}\}}_{0} - c_{i\sigma}^\dagger \underbrace{\{c_{j\sigma'}^\dagger, c_{i\sigma}\}}_{\delta_{ji}\delta_{\sigma\sigma'}} c_{k\sigma'} \tag{A.32}$$
$$= \delta_{ki}\delta_{\sigma\sigma'} c_{j\sigma'}^\dagger c_{i\sigma} - \delta_{ji}\delta_{\sigma\sigma'} c_{i\sigma}^\dagger c_{k\sigma'}.$$

The second term is just a commutation relation of two density operators $[\hat{n}_{j\sigma'}, \hat{n}_{i\sigma}]$. This will just return the number density $n_{i\sigma}$ and $n_{j\sigma'}$ at the two states, and since the N−particle state will only be scaled by $n_{i\sigma}n_{j\sigma'}$, the operators trivially commute,

$$\left[c_{j\sigma'}^\dagger c_{j\sigma'}, c_{i\sigma}^\dagger c_{i\sigma}\right] = 0. \tag{A.33}$$

For the third term, using the fermionic anti-commutation relation $\{c_{j\sigma}^\dagger, c_{j\bar\sigma}\} = 0$ and $\{c_{j\sigma}, c_{j\bar\sigma}\} = 0$, we then can transform the commutation relation as the commutation of $\hat{n}_{i\sigma}$ with $\hat{n}_{j\uparrow}\hat{n}_{j\downarrow}$, which is again, trivially zero,

$$\left[c_{j\uparrow}^\dagger c_{j\downarrow}^\dagger c_{j\downarrow} c_{j\uparrow}, c_{i\sigma}^\dagger c_{i\sigma}\right] = 0. \tag{A.34}$$

Appendix B

Ginzburg-Landau theory and the coherence length

In statistical mechanics, all thermodynamic properties of a system can principally be extracted from the partition function Z, which is calculated by summing over all possible states in some microscopic Hamiltonian $\mathcal{H}_{mic}$,

$$Z = \text{tr}[\exp(-\beta\mathcal{H}_{\text{mic}})] = \int \mathcal{D}\Delta(\mathbf{r})\mathcal{W}[\Delta(\mathbf{r})] \tag{B.1}$$

The right hand side of the equation is the integration over all allowed configurations of the order parameter $\mathcal{D}\Delta(\mathbf{r})$, weighted with probability $\mathcal{W}[\Delta(\mathbf{r})]$. In superconductivity one integrates over a d-dimensional space $\mathbf{r} \in \mathbb{R}^d$ and a complex order parameter $\Delta \in \mathcal{C}$.

In phase transitions, the minimization of the free energy density f is a crucial thermodynamic variable to analyze,

$$fV = -\beta^{-1}\ln Z \tag{B.2}$$

where V is the system size. While it is theoretically possible to calculate such partition function, the use of phenomenological parameters may ease the process. Furthermore, using saddle point approximation, one can replace the entire integral in Eq. B.1 with the maximum value of the integrand assuming that the order parameter varies slowly in space. This corresponds to the most probable configuration of Δ [38]. This leads to the Ginzburg-Landau free energy density function, with a temperature-dependent phenomenological parameter α, β, and the normal state free energy f_{n0}.

$$f = f_{n0} + \alpha|\Delta|^2 + \frac{\beta}{2}|\Delta|^4 + \frac{1}{2m^*}\left|\left(\frac{\hbar}{i}\nabla - \frac{e}{c}\mathbf{A}\right)\Delta\right|^2 + \frac{h^2}{8\pi} \tag{B.3}$$

The above can also be seen as a power expansion of $|\Delta|^2$ to the second order. The third term possesses the canonical momentum in a electromagnetic field due to quantum mechanics, while h^2 takes into account the energy of an external magnetic field. Through this, one may determine the minimization of free energy through $f - f_{n0}$.

There are several interesting observation that one can extract from Ginzburg-Landau free energy as shown by Tinkham. Assuming the absence of fields and gradients, we
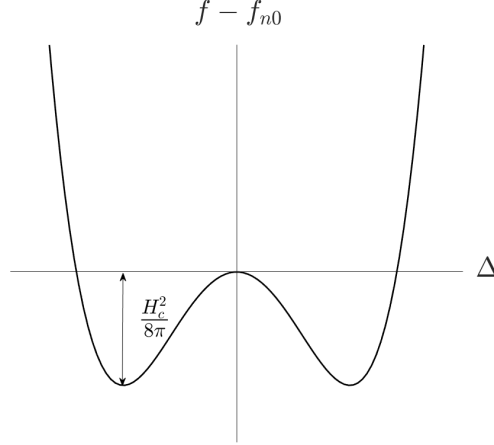
Figure B.1: Ginzburg-Landau free energy for $\alpha > 0$.

are left with the term,

$$f - f_{n0} = \alpha|\Delta|^2 + \frac{\beta}{2}|\Delta|^4 \tag{B.4}$$

From this, one finds that for $\alpha \geq 0$ the minimum free energy occurs at $|\Delta|^2_{\min} = 0$, which is trivially the normal state. A more interesting case lies for $\alpha < 0$, where one obtains a minimum whereby $f < f_n$ at $|\Delta|^2_{\min} = -\frac{\alpha}{\beta}$ (see Fig. B.1).

Since we have assumed that the order parameter varies slowly, we know that it is the magnetic term $\frac{h^2}{8\pi}$ that plays a big role to fulfill the difference in free energy. With this, it can be deduced, that the gap between the free energies correspond to the critical field,

$$\frac{H_c^2}{8\pi} = f - f_{n0} \tag{B.5}$$

This information will be crucial for chapter 4 to estimate the critical field at which a phase transition occurs.

Another observation one can discuss, is the minimization of the free energy along the order parameter, to obtain the well-knowned Ginzburg-Landau equations.

$$\alpha\Delta + \beta|\Delta|^2\Delta + \frac{1}{2m^*}\left(\frac{\hbar}{i}\nabla - \frac{e}{c}\mathbf{A}\right)^2\Delta = 0 \tag{B.6}$$

For simplicity, one can treat this differential equation in one-dimensional space under $\mathbf{A} = 0$. Normalization of the order parameter with $\Psi = \frac{\Delta}{\Delta_{\min}}$ gives us,

$$\xi^2\frac{d^2}{dx^2}\Psi + \Psi - \Psi^3 = 0, \quad \xi^2 = \frac{\hbar^2}{2m^*|\alpha(T)|}. \tag{B.7}$$

From the equation above, we have obtained another characteristic parameter ξ called the coherence length. This length determines the spatial variation at which an order parameter increases. Naively speaking, the coherence length then defines the length scale at which electrons can play a role in the superconducting state [15].

Appendix C

Figures and Calculations
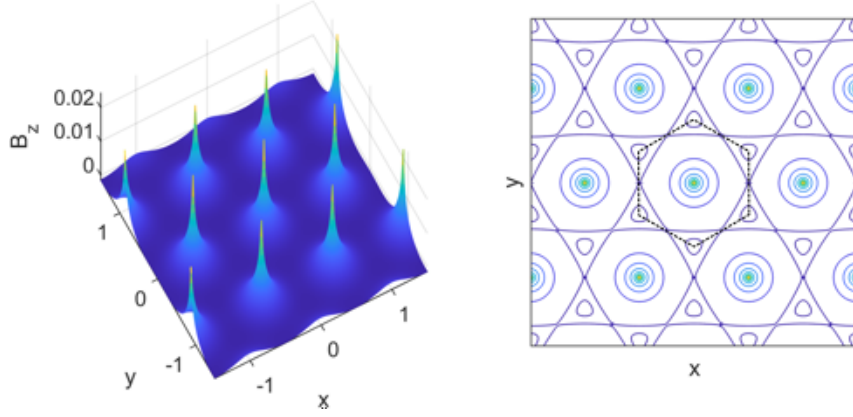
C.1 Magnetic field distribution of vortex lattice

Figure C.1: Field distribution (left) of a hexagonal lattice using the Fourier series with its respective contour plot (right) where saddle points are indicated by intersecting contour lines. A unit cell is shown as dotted lines. $\lambda = 1$. $B_{\mathrm{a}} = 1$.
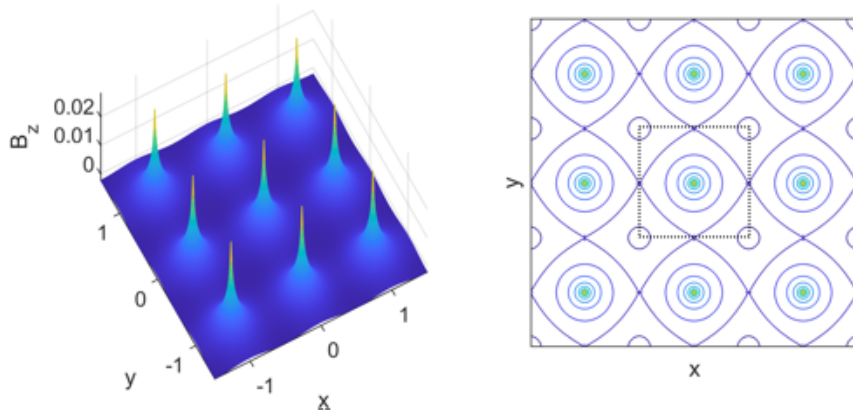

Figure C.2: Field distribution (left) of a square lattice using the Fourier series with its respective contour plot (right) where saddle points are indicated by intersecting contour lines. A unit cell is shown as dotted lines. $\lambda = 1$. $B_{\mathrm{a}} = 1$.

C.2 Visualization convergence of the vortex state

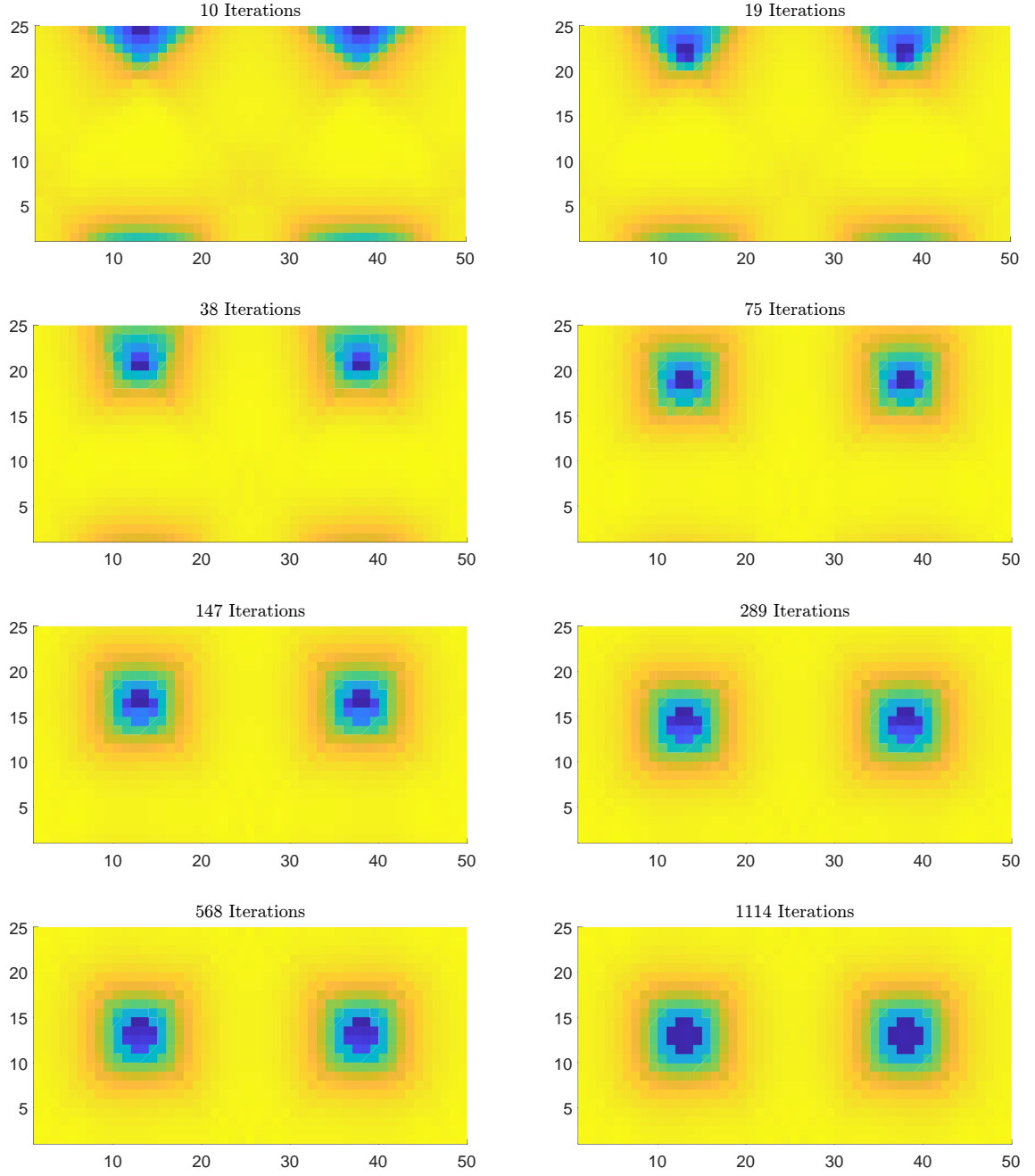The following is the convergence of gap parameter forming the vortex state.

Figure C.3: Convergence of gap parameter with numbers of iterations. $t = 1$, $V = -1.95t$, $B = \frac{2\Phi_0}{L_x L_y}$.

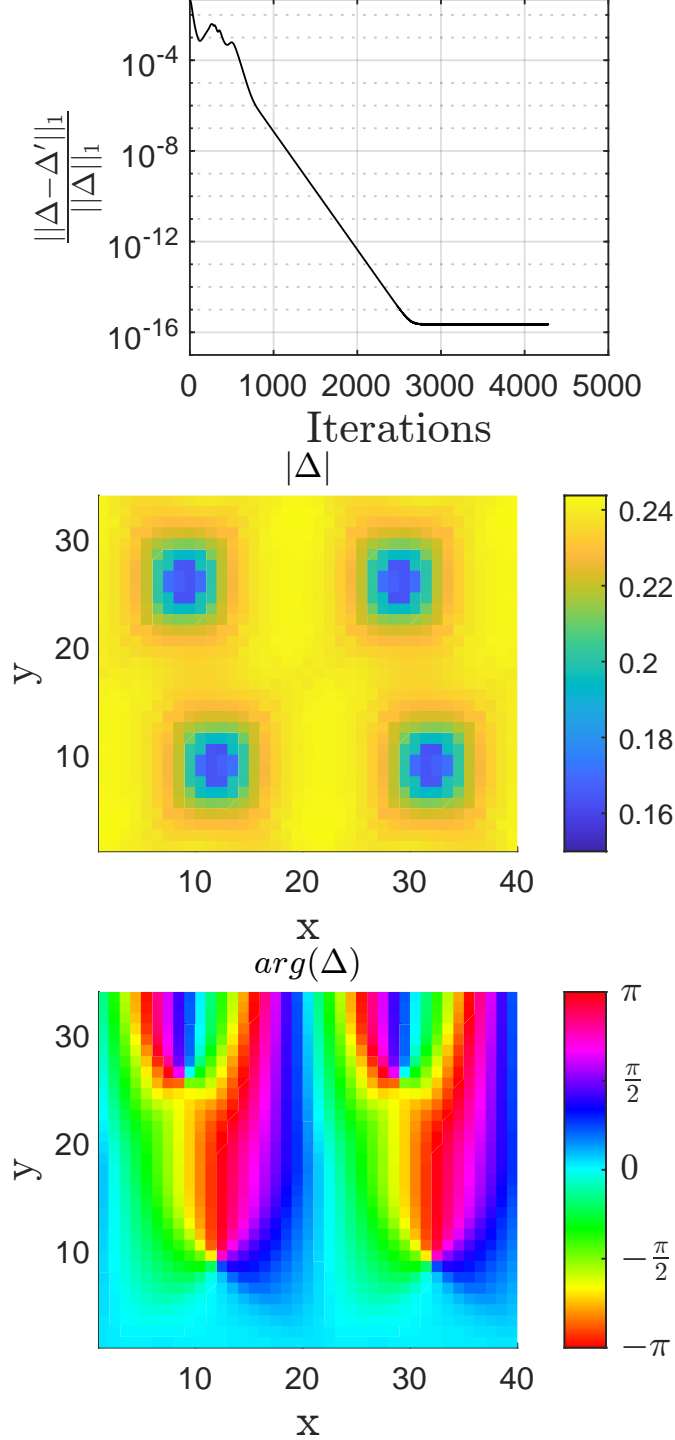# C.3   Preliminary calculation of the hexagonal vortex lattice

Figure C.4: Preliminary calculation of the hexagonal vortex lattice. The magnetic unit cell with $L_x \times L_y$ lattice points is set in such a way that it ideally accomodates a hexagonal lattice structure of the vortex. Note that this is not yet converged.

Bibliography

[1] Kamerlingh Onnes. Further experiments with liquid helium. O. On the measurement of very low temperatures XXV. The determination of the temperatures which are obtainded with liquid helium, especially in connection with measurements of the vapour pressure of helium. *Proceedings of the Koninklijke Nederlandse Akademie van Wetenschappen*, 18 I:493–507, 1915.

[2] J. File and R. G. Mills. Observation of Persistent Current in a Superconducting Solenoid. *Physical Review Letters*, 10:93–96, 2 1963.

[3] W. Meissner and R. Ochsenfeld. Ein neuer Effekt bei Eintritt der Supraleitfähigkeit. *Die Naturwissenschaften*, 21:787–788, 11 1933.

[4] Martin Durrani and Paul Michael Grant. Down the path of least resistance. *Physics World*, pages 18–22, 4 2011.

[5] Kazue Matsuyama and Jeff Greensite. Nature of symmetry breaking in the superconducting ground state. *Physical Review B*, 100:184513, 11 2019.

[6] W.J. De Haas and J.M. Casimir-Jonker. Untersuchungen Über den Verlauf des Eindringens Eines Transversalen Magnetfeldes in Einen Supraleiter. *Physica*, 1:292–296, 1 1934.

[7] L. V. Shubnikov, V. I. Khotkevich, Yu. D. Shepelev, and Yu. N. Ryabinin. Magnetic properties of superconducting metals and alloys. *Zh. Eksper. Teor. Fiz*, 7:221–237, 1937.

[8] A.A. Abrikosov. The magnetic properties of superconducting alloys. *Journal of Physics and Chemistry of Solids*, 2:199–208, 1 1957.

[9] Fritz London. *Superfluids, Macroscopic Theory of Superconductivity Vol. 1.* Dover Publications, Inc., New York, 2nd edition, 1961.

[10] Bascom S. Deaver and William M. Fairbank. Experimental Evidence for Quantized Flux in Superconducting Cylinders. *Physical Review Letters*, 7:43–46, 7 1961.

[11] W. H. Kleiner, L. M. Roth, and S. H. Autler. Bulk Solution of Ginzburg-Landau Equations for Type II Superconductors: Upper Critical Field Region. *Physical Review*, 133:A1226–A1227, 3 1964.

[12] U. Essmann and H. Träuble. The direct observation of individual flux lines in type II superconductors. *Physics Letters A*, 24:526–527, 5 1967.

[13] Henrik Bruus and Karsten Flensberg. *Many-body quantum theory in condensed matter physics*. Oxford University Press, New York, 2002.

[14] Fritz London and Heinz London. The electromagnetic equations of the supraconductor. *Proceedings of the Royal Society of London. Series A - Mathematical and Physical Sciences*, 149:71–88, 3 1935.

[15] Michael Tinkham. *Introduction to Superconductivity*. McGraw-Hill, Inc., New York, 2nd edition, 1996.

[16] D. Bohm. Note on a Theorem of Bloch Concerning Possible Causes of Superconductivity. *Physical Review*, 75:502–504, 2 1949.

[17] Steven H. Simon. *The Oxford Solid State Basics*. Oxford University Press, Oxford, 1st edition, 2013.

[18] Alexander Altland and Ben Simons. *Condensed Matter Field Theory*. Cambridge University Press, New York, 2nd edition, 2010.

[19] B. A. McKinnon and T. C. Choy. Significance of nonorthogonality in tightbinding models. *Physical Review B*, 52:14531–14538, 11 1995.

[20] J. M. Luttinger. The Effect of a Magnetic Field on Electrons in a Periodic Potential. *Physical Review*, 84:814–817, 11 1951.

[21] Rudolf Peierls. On the Theory of the Diamagnetism of Conduction Electrons. In *World Scientific Series in 20th Century Physics : Selected Scientific Papers of Sir Rudolf Peierls*, pages 97–120. 4 1997.

[22] Cecilie Hermansen. *Vortices in s-Wave Superconductors A Numerical Study of the Bogoliubov-de Gennes Equations*. Bachelor's thesis, Niels Bohr Institute, Copenhagen, 6 2018.

[23] Douglas R. Hofstadter. Energy levels and wave functions of Bloch electrons in rational and irrational magnetic fields. *Physical Review B*, 14:2239–2249, 9 1976.

[24] Monika Aidelsburger. *Artificial gauge fields with ultracold atoms in optical lattices*. PhD thesis, Ludwig-Maximilians-Universität München, München, 12 2015.

[25] John Boyd Ketterson and S. N. Song. *Superconductivity*. Cambridge University Press, Cambridge, 1999.

[26] Christine Völlinger. *Superconductor Magnetization Modeling for the Numerical Calculation of Field Errors in Accelerator Magnets*. PhD thesis, Technischen Universität Berlin, Berlin, 10 2003.

[27] C.J. Gorter. The Two Fluid Model for Superconductors and Helium II. In *Progress in Low Temperature Physics*, volume 1, chapter 1, pages 1–16. Elsevier, 5 1955.

[28] Carolyn L. Phillips, Tom Peterka, Dmitry Karpeyev, and Andreas Glatz. Detecting vortices in superconductors: Extracting one-dimensional topological singularities from a discretized complex scalar field. *Physical Review E*, 91:023311–undefined, 2 2015.

[29] J. Bardeen, L. N. Cooper, and J. R. Schrieffer. Theory of Superconductivity. *Physical Review*, 108:1175–1204, 12 1957.

[30] Philip Whittlesea. *Unconventional superconductivity: A theoretical study of equal-spin triplet-pairing in LaNiGa 2 and the potential application of topological transitions to quench prevention.* PhD thesis, University of Kent, Kent, 9 2019.

[31] Charles P. Poole Jr., Horatio A. Farach, Richard J. Creswick, and Ruslan Prozorov. *Superconductivity.* Elsevier, Amsterdam, 2nd edition, 2007.

[32] Florian Loder. *Magnetic Flux Periodicities and Finite Momentum Pairing in Unconventional Superconductors.* PhD thesis, Universität Augsburg, Augsburg, 11 2009.

[33] Elena Otilia, Diana Enescu, Mihail-Florin Stan, and Marcel Ionel. Finite Element Analysis of Stationary Magnetic Field. In Farzad Ebrahimi, editor, *Finite Element Analysis - New Trends and Developments*, chapter 5, pages 101–129. InTech, 10 2012.

[34] Sheng Ran, I. Lin Liu, Yun Suk Eo, Daniel J. Campbell, Paul M. Neves, Wesley T. Fuhrman, Shanta R. Saha, Christopher Eckberg, Hyunsoo Kim, David Graf, Fedor Balakirev, John Singleton, Johnpierre Paglione, and Nicholas P. Butch. Extreme magnetic field-boosted superconductivity. *Nature Physics*, 15:1250–1254, 12 2019.

[35] Yuki Nagai, Yasushi Shinohara, Yasunori Futamura, Yukihiro Ota, and Tetsuya Sakurai. Numerical construction of a low-energy effective Hamiltonian in a self-consistent Bogoliubov-de Gennes approach of superconductivity. *Journal of the Physical Society of Japan*, 82:094701, 3 2013.

[36] George B Arfken and Hans J Weber. *Mathematical Methods for Physicists.* Elsevier Academic Press, 6th edition, 2005.

[37] J. Douglas Faires and Richard L. Burden. *Numerical Methods.* Brooks Cole, 3rd edition, 2002.

[38] Mehran Kardar. *Statistical Physics of Fields.* Cambridge University Press, Cambridge, 2007.